We are IntechOpen, the world's leading publisher of Open Access books Built by scientists, for scientists

4,800
Open access books available

122,000
International authors and editors

135M
Downloads

Our authors are among the

154
Countries delivered to

TOP 1%
most cited scientists

12.2%
Contributors from top 500 universities

CLARIVATE ANALYTICS BOOK CITATION INDEX INDEXED

WEB OF SCIENCE™

Selection of our books indexed in the Book Citation Index in Web of Science™ Core Collection (BKCI)

Interested in publishing with us?
Contact book.department@intechopen.com

Numbers displayed above are based on latest data collected.
For more information visit www.intechopen.com

1

Using Infrared Spectroscopy to Identify New Amorphous Phases – A Case Study of Carbonato Complex Formed by Mechanochemical Processing

Tadej Rojac[1], Primož Šegedin[2] and Marija Kosec[1]
[1]*Jožef Stefan Institute*
[2]*Faculty of Chemistry and Chemical Technology,*
University of Ljubljana
Slovenia

1. Introduction

1.1 Mechanochemistry and high-energy milling

Since the first laboratory experiments of M. Carey Lea and the original definition by F. W. Ostwald at the end of the 19th century, mechanochemistry, a field treating chemical changes induced in substances as a result of applied mechanical stress, has been evolved as an important area of chemistry from the viewpoint of both the fundamental research and applications (Takacs, 2004; Boldyrev & Tkačova, 2000). Whereas the fundamentals of mechanochemistry are still being extensively explored, the mechanical alloying, a powder metallurgy process involving ball milling of particles under high-energy impact conditions, met the commercial ground as early as in 1966 and was used to produce improved nickel- and iron-based alloys for aerospace industry (Suryanarayana et al., 2001). In addition to metallurgy, the science and technology of mechanochemical processes are continuously developing within various other fields, including ceramics processing, processing of minerals, catalysis, pharmaceutics, and many others.

Due to simplicity and technological reasons, the most common way to apply mechanical stress to a solid is via ball-particle collisions in a milling device. This is often referred to as the "high-energy milling" technique. What distinguish this method from the classical "wet ball-milling", used primarily for reducing particle size and/or mixing components, is that a powder or mixture of powders is typically milled in liquid-free conditions; under such circumstances, a larger amount of the kinetic energy of a moving ball inside a grinding bowl is transferred to the powder particles during collisions; this is also the origin of the term "high-energy" milling. Owing to the feasibility to conduct chemical reactions by high-energy milling, an often used term in the literature is "mechanochemical synthesis".

To carry out mechanochemical processes, various types of milling devices are used, including shaker, planetary, horizontal, attrition mill, etc. (Lu & Lai, 1998). One of the most

used, in particular for research purposes, is the planetary ball mill (Fig. 1a). A schematic view of the ball motion inside a grinding bowl of a planetary mill is illustrated in Fig. 1b. This characteristic ball motion results from two types of rotations: i) rotation of the grinding bowl around its center and ii) rotation of the supporting disc to which the bowls are attached; the two rotational senses are opposite (see Fig. 1b). In such a rotational geometry, the forces acting on the milling balls result into a periodical ball movement, illustrated by arrows in Fig. 1b, during which, when certain conditions are met, the balls are detached from the bowl's internal surface, colliding onto the powder particles on the opposite side. Even if simplified, the mathematical model derived from such an idealized ball movement agreed well with the experimental measurements of power consumption during milling (Burgio et al., 1991; Iasonna & Magini, 1996). In addition, this periodical movement was confirmed by numerical simulations (Watanabe et al., 1995a) and high-speed video camera recordings (Le Brun et al., 1993).

The high energy released during ball-powder collisions leads to various phenomena in the solid; this includes creation of a large amount of defects in the crystal structure, amorphization or complete loss of long-range structural periodicity, plastic and elastic deformation of particles, decrease of particle size down to the nanometer scale, increase of specific surface area of the powders, polymorphic transitions and even chemical reactions (Fig. 1c). Such changes result in distinct powder properties. The so-called mechanochemical reactions, which take place directly during the milling process without any external supply of thermal energy, make the method particularly interesting and distinguished from other conventional synthesis methods, which are typically based upon thermally driven reactions.

Due to their complexity, understanding mechanochemical reactions and the underlying mechanisms is a difficult task. In addition to local heating, provided by the high-energy collisions, modelling of the high-energy milling process revealed a large increase of pressure at the contact area between two colliding milling balls, which can reach levels of up to several GPa. It should be noted that both temperature and pressure rise are realized in tenths of microseconds, an estimated duration of a collision, illustrating the non-equilibrium nature of the mechanochemical process (Maurice & Courtney, 1990). Actually, during high-energy collisions the powder particles are subjected to a combination of hydrostatic and shear stress components, which further complicate the overall picture, even in apparently simple cases, such as polymorphic phase transitions. It was shown, for example, that conventional thermodynamic phase diagrams cannot be applied for polymorphic phase transitions realized during high-energy milling (Lin & Nadiv, 1979). In fact, the classical hydrostatic-pressure–temperature (p-T) phase diagram, e.g., in the case of a polymorphic transition between litharge and massicot forms of PbO, is considerably altered by introducing the shear component into the calculations; a two-phase field region appears in the phase diagram, suggesting co-existence of the two polymorphs, rather than a sharp transition line characteristic for the conventional PbO p-T diagram. This might explain the often observed co-existence of two polymorphic modifications upon prolonged milling when "steady-state" milling conditions are reached (Lin & Nadiv, 1979; Iguchi & Senna, 1985). The influence of shear stress and local temperature rise on more complex mechanochemical reactions are still subject of intensive discussions.

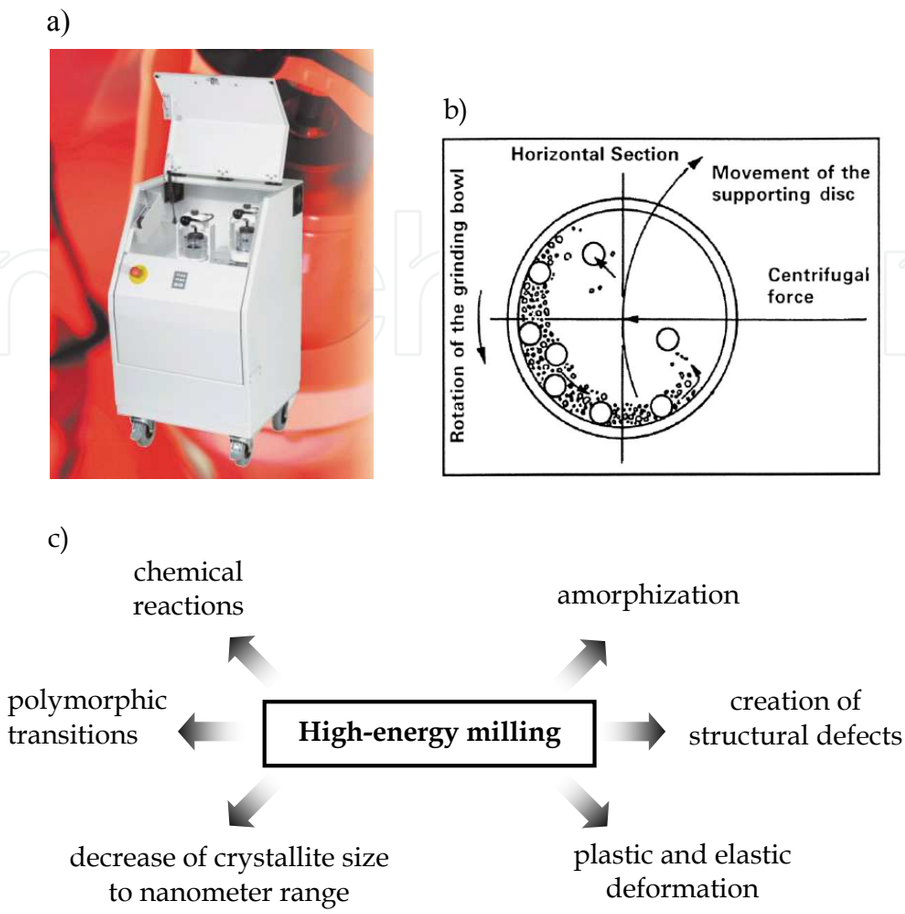

Fig. 1. a) Laboratory-scale planetary mill Fritsch Pulverisette 4, b) schematic representation of the movement of milling balls in a planetary mill (from Suryanarayana, 2001) and c) characteristic phenomena taking place in the solids as a result of high-energy collisions.

1.2 Mechanochemical synthesis of complex ceramic oxides and underlying reaction mechanisms

Mechanochemical synthesis (or high-energy milling assisted synthesis) has been found particularly useful for the synthesis of ceramic oxides with complex chemical composition, ranging from ferroelectric, magnetic and multiferroic oxides to oxides exhibiting semiconducting and catalytic properties. For an overview of the research activity in this field the reader should consult Kong et al. (2008) and Sopicka-Lizer (2010).

Whereas, in general, extensive literature data can be found on the mechanochemical synthesis of complex oxides, only limited studies are devoted to the understanding of mechanochemical reaction mechanisms. Primarily driven by the need to enrich our fundamental knowledge of mechanochemistry, the studies of reaction mechanisms have also been found to be essential in order to efficiently design a mechanochemical process, which includes the selection of milling parameters, milling regime, etc. (Rojac et al., 2010).

One of the main difficulties in analyzing the complex mechanisms of mechanochemical reactions is the identification of amorphous phases, which are metastable and appear often transitional with respect to the course of the reaction. To illustrate an example, we present in Fig. 2 the mechanochemical synthesis of $KNbO_3$ from a powder mixture of K_2CO_3 and Nb_2O_5 (Rojac et al., 2009). In the first 90 hours of milling, the initial crystalline K_2CO_3 and Nb_2O_5 (Fig. 2a, 0 h) are transformed into an amorphous phase, characterized by two broad "humps" centred at around 29° and 54° 2-theta (Fig. 2a, 90 h). The formation of the amorphous phase was confirmed by transmission electron microscopy (TEM), i.e., an amorphous matrix was observed with embedded nanocrystalline particles of Nb_2O_5 (Fig. 2b), which is consistent with the X-ray diffraction (XRD) pattern (Fig. 2a, 90 h). Further milling from 90 to 350 hours resulted in the crystallization from the amorphous phase; this is evident from the appearance of new peaks after 150 and 350 hours of milling, which were assigned to various potassium niobate phases with different K/Nb molar ratio (Fig. 2a, 150 and 350 h). Therefore, the amorphous phase represents a transitional phase of the reaction. In addition, comparison of the 90-hours milled K_2CO_3–Nb_2O_5 mixture (Fig. 2a, 90 h) with the

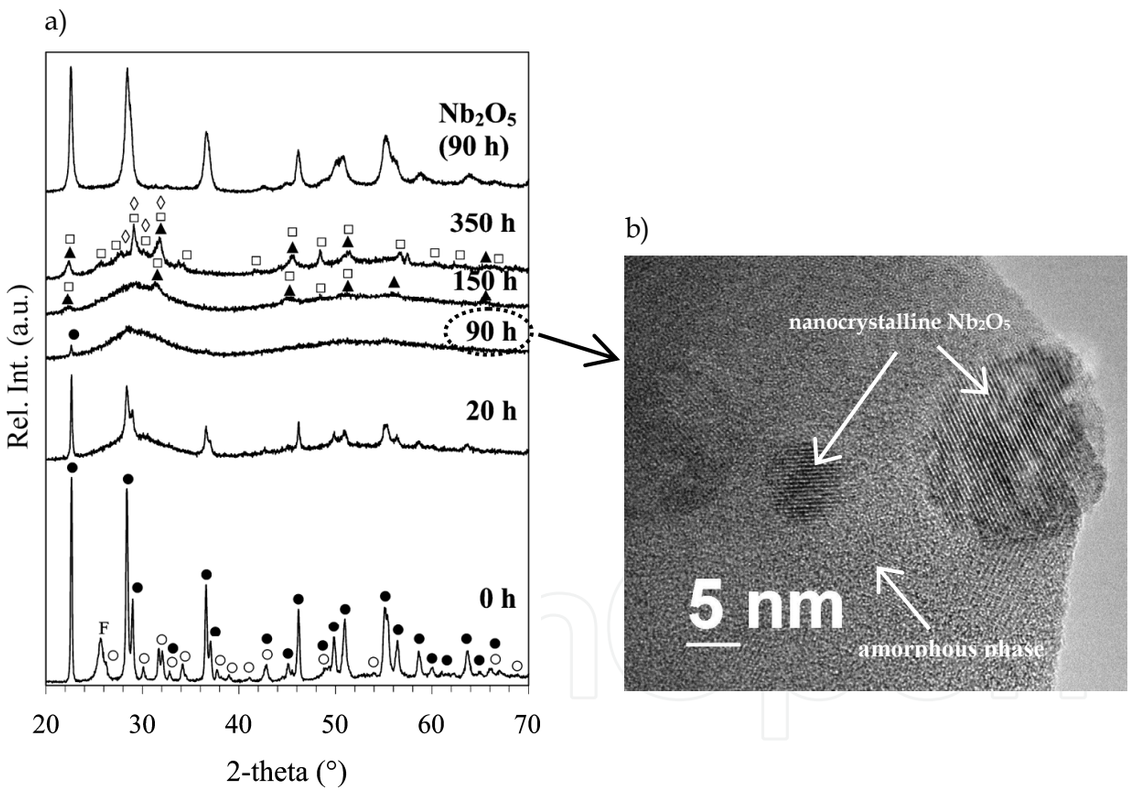

Fig. 2. a) XRD patterns of K_2CO_3–Nb_2O_5 powder mixture after high-energy milling for 20, 90, 150 and 350 hours. The non-milled mixture is denoted as "0 h". The pattern of the 90-hours-separately-milled Nb_2O_5 is added for comparison. In order to prevent adsorption of water during XRD measurements, a polymeric foil was used to cover the non-milled powder mixture. b) TEM image of the K_2CO_3–Nb_2O_5 powder mixture after high-energy milling for 90 hours. Notations: K_2CO_3 (○, PDF 71-1466), Nb_2O_5 (●, PDF 30-0873), $KNbO_3$ (▲, PDF 71-0946), $K_6Nb_{10.88}O_{30}$ (□ , PDF 87-1856), $K_8Nb_{18}O_{49}$ (◊, PDF 31-1065), polymeric foil (F); "h" denotes milling hours (from Rojac et al., 2009).

90-hours separately milled Nb_2O_5 (Fig. 2a, Nb_2O_5 90 h), revealed a much larger degree of amophization of Nb_2O_5 when co-milled with K_2CO_3; note the considerably weaker Nb_2O_5 peaks and higher XRD background in the case of the mixture as compared to separately milled Nb_2O_5. This suggests that the amorphization of Nb_2O_5 is not a consequence of the high-energy impacts only, but has its origin in the mechanochemical interaction with the carbonate. It should be emphasized that this is not an isolated case; examples involving transitional amorphous phases can also be found during mechanical alloying of mixture of metals (El-Eskandarany et al., 1997). Finally, a nucleation-and-growth mechanism from amorphous phase was recently proposed as a general concept to explain the mechanochemical synthesis of a variety of complex oxides, such as $Pb(Zr_{0.52}Ti_{0.48})O_3$, $Pb(Mg_{1/3}Nb_{2/3})O_3$, $Pb(Zn_{1/3}Nb_{2/3})O_3$, etc. (Wang et al., 2000a, 2000b; Kuscer et al., 2006). In order to understand mechanochemical reactions, it is thus indispensable to analyze more closely the transitional amorphous phase.

It is clear from the above considerations that the most often used and widely reported XRD analysis becomes insufficient to provide detailed information about amorphous phases. The benefits of in-depth studies of mechanochemical reaction mechanisms by selection of appropriate analytical tools, able to provide data on a short-range (local) structural scale, such as nuclear magnetic resonance (NMR), X-ray photoelectron spectroscopy (XPS), electron paramagnetic resonance (EPR) spectroscopy, infrared spectroscopy (IR), Raman spectroscopy, etc., were demonstrated by the pioneering work of Senna, Watanabe and co-workers (Watanabe et al., 1996, 1997; Senna, 1997). In those cases, the synthesis of selected complex oxide systems have been studied from starting mixtures comprising typically hydroxide and oxide compounds; extensive data on these studies can be found in Avvakumov et al. (2001).

Mechanochemical processing has recently provided important improvements in the synthesis of ceramic materials in the family of alkaline niobates tantalates, a rich group of materials exhibiting wide applicability; this includes $KTaO_3$ and $(K,Na,Li)(Nb,Ta)O_3$ (KNLNT), which are considered as promising materials for dielectric (microwave) and piezoelectric applications, respectively (Glinsek et al., 2011; Tchernychova et al., 2011; Rojac et al., 2008a, 2010). Since alkali carbonates are the most frequently used as starting alkali compounds, it naturally became of interest to understand in more details the mechanochemical reaction mechanisms in which carbonate ions (CO_3^{2-}) are involved. The results of these studies carry important practical consequences. For example, in the case of the synthesis of the complex KNLNT solid solution, it was demonstrated that the identification of the reaction mechanism during mechanochemical processing is a key step leading to highly homogeneous KNLNT ceramics with excellent piezoelectric response. After identifying an intermediate amorphous carbonato complex, to which the present chapter is particularly devoted, it was found that a homogeneous KNLNT can only be obtained by providing the formation of this complex during the high-energy milling step. In other words, milling conditions that did not lead to the formation of the carbonato complex, e.g., milling in the "friction" mode instead of the "friction+impact" mode, resulted into considerable Ta-inhomogeneities and, consequently, to a reduced piezoelectric response (Rojac et al., 2010).

In this chapter we present an overview of the studies of reaction mechanisms in systems comprising CO_3^{2-} ions. The chapter aims primarily at showing the importance of combining various analytical methods, including quantitative XRD analysis, thermal analysis and

infrared spectroscopy, to obtain an overall picture of a complex reaction mechanism, such as the one encountered during mechanochemical processing. The first part of the chapter is devoted to the synthesis of $NaNbO_3$ from a mixture of Na_2CO_3 and Nb_2O_5. After demonstrating the feasibility of synthesizing $NaNbO_3$ directly by high-energy milling, we show systematically how a mechanism can be revealed by a built-up of data from various analytical methods. The focus is to gain insight into the amorphous phase, which represents a transitional phase in the synthesis of $NaNbO_3$. In the second part of the chapter we will extent the studies to other systems based on sodium carbonate, i.e., Na_2CO_3–M_2O_5 (M = V, Nb, Ta). The transition-metal oxides were selected through the 5th group of the periodic table to allow systematic comparisons and propose potentially a general reaction mechanism.

2. Mechanochemical reaction mechanism in the Na_2CO_3–Nb_2O_5 system studied by a combination of quantitative X-ray diffraction, thermal and infrared spectroscopy analysis

2.1 Quantitative X-ray diffraction analysis

The mechanochemical synthesis of $NaNbO_3$ from a Na_2CO_3–Nb_2O_5 mixture was followed by XRD analysis. Fig. 3 shows the XRD patterns of the Na_2CO_3–Nb_2O_5 mixture after selected milling times. The pattern of the non-milled mixture (Fig. 3, 0 h), which is a homogenized mixture of Na_2CO_3 and Nb_2O_5 powders just before mechanochemical treatment, can be fully indexed with the initial monoclinic Na_2CO_3 and orthorhombic Nb_2O_5 (Fig. 3, 0 h). The first 5 hours of high-energy milling are characterized by broaden peaks of the two reagents together with reduced peak intensity (Fig. 3, 5 h). After 40 hours of milling Na_2CO_3 was not observed anymore in the mixture, whereas traces of the newly formed $NaNbO_3$ were first detected (Fig. 3, 40 h). Further milling from 40 to 400 h leaded to a progressive disappearance of Nb_2O_5 from the mixture at the expense of the growing $NaNbO_3$. Note the long milling time, i.e., 400 hours, needed to obtain the final $NaNbO_3$ free of any reagents (Fig. 3, 400 h). The low rate of the reaction between Na_2CO_3 and Nb_2O_5 resulted from the mild milling conditions, which were applied intentionally in order to enable a careful analysis of the individual reaction stages. It should be noted, however, that more intensive milling, resulting into $NaNbO_3$ after 32 hours of milling, did not change qualitatively the course of the reaction (for details see Rojac et al., 2008b). The results of the XRD analysis from Fig. 3 confirm the mechanochemical formation of $NaNbO_3$ according to the following reaction:

$$Na_2CO_3 + Nb_2O_5 \rightarrow 2NaNbO_3 + CO_2 \quad (1)$$

In order to obtain a more quantitative picture of the mechanochemical reaction, we performed a quantitative XRD phase analysis using the Rietveld refinement method. In addition to the amount of the crystalline phases, i.e., Na_2CO_3, Nb_2O_5 and $NaNbO_3$, we determined also the contribution from the XRD background, which we denoted as "XRD-amorphous" phase. This was done using an internal standard method; details of the method can be found in Kuscer et al. (2006) and Rojac et al. (2008b).

The results of the refinement analysis in terms of the amounts of Na_2CO_3, Nb_2O_5, $NaNbO_3$ and XRD-amorphous phase as a function of milling time are shown in Fig. 4. The amounts

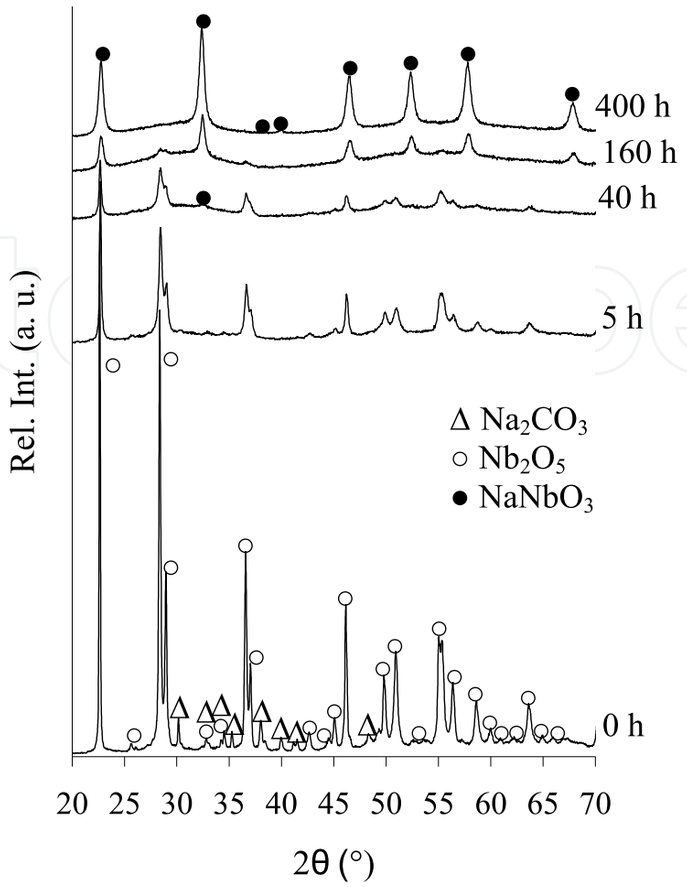

Fig. 3. XRD patterns of Na_2CO_3–Nb_2O_5 powder mixture after high-energy milling for 5, 40, 160 and 400 hours. The non-milled mixture is denoted as "0 h". Notations: Na_2CO_3 (Δ, PDF 19-1130), Nb_2O_5 (○, PDF 30-0873) and $NaNbO_3$ (●, PDF 33-1270); "h" denotes milling hours (from Rojac et al., 2008b).

of both Na_2CO_3 and Nb_2O_5 decrease with milling time (Fig. 4a). While Nb_2O_5 persists in the mixture up to 280 hours (Fig. 4a, closed rectangular), Na_2CO_3 is no longer detected after 20 hours of milling (Fig. 4a, open rectangular). The amount of the XRD-amorphous phase rapidly increases in the initial part of the reaction, reaching a maximum of 91% after 110 hours of milling, after which it decreases with further milling. Note the constant amount of the XRD-amorphous phase after reaching 600 hours of milling. The formation of $NaNbO_3$ follows a sigmoidal trend: at the beginning of the reaction the formation rate is low, after which it increases and slows down again in the final part of the reaction (Fig. 4b, open circles). Similarly like the XRD-amorphous phase, no differences in the amount of $NaNbO_3$ are observed with milling from 600 to 700 hours, suggesting a constant $NaNbO_3$-to-amorphous-phase mass ratio upon prolonged milling.

From the quantitative analysis, shown in Fig. 4, an important observation can be derived by looking more closely at the initial stage of the reaction. An enlarged view of this part of the reaction is shown as inset in Fig. 4b. Here, we can see that in the initial 20 hours of milling, during which no $NaNbO_3$ was detected, a large amount, i.e., 73%, of the amorphous phase was formed. Only subsequently, i.e., after 40 hours of milling, $NaNbO_3$ was firstly detected.

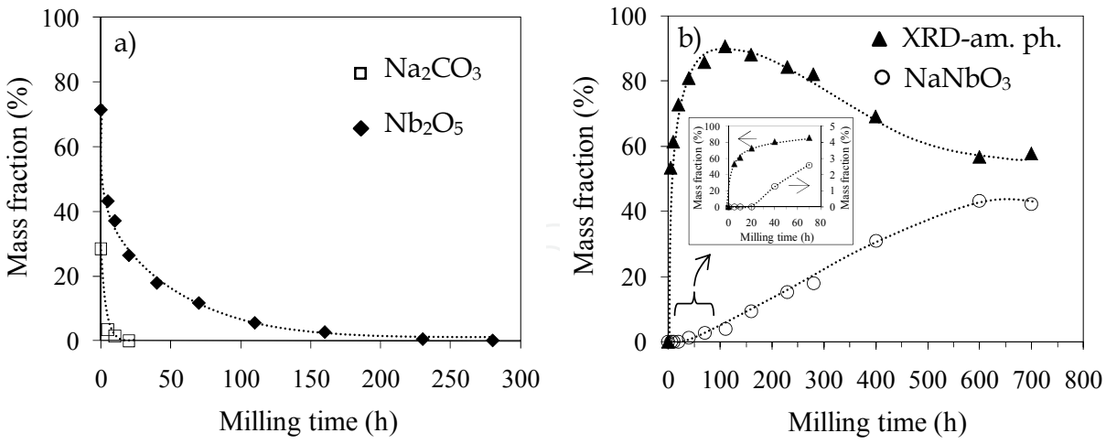

Fig. 4. Fractions of crystalline phases (Na_2CO_3, Nb_2O_5 and $NaNbO_3$) and XRD-amorphous phase, determined by Rietveld refinement analysis, as a function of milling time. a) Na_2CO_3 and Nb_2O_5, b) $NaNbO_3$ and XRD-amorphous phase. The inset of b) shows an enlarged view of the curves in the initial 80 hours of milling. The lines are drawn as a guide for the eye (from Rojac et al., 2008b).

From this simple observation we can infer that $NaNbO_3$ is not formed directly, like assumed by equation 1, but through an intermediate amorphous phase. The transitional nature of the amorphous phase is further confirmed by the maximum in its amount after 110 hours of milling. Moreover, literature data go in favour of our conclusions. In fact, based on studies of the kinetics, the sigmoidal trend, like that observed in the case of $NaNbO_3$ (Fig. 4b, open circles), is characteristic for multistep mechanochemical processes, such as the amorphization of a mixture of metals, where the phase transformation requires two or more impacts on the same powder fraction. In contrast, continuously decelerating processes, described by asymptotic kinetics, are typical for the amorphization of single-phase compounds, such as intermetallics, where the structure is already altered after the first impact (Delogu & Cocco, 2000; Cocco et al., 2000; Delogu et al., 2004). Therefore, independently of the analysis on the XRD-amorphous phase, the sigmoidal-like trend in the formation of $NaNbO_3$ (Fig. 4b, open circles) suggests that the niobate is formed via a transitional phase.

In addition to the XRD-amorphous phase, we shall look at the changes induced in the Na_2CO_3 in the initial part of milling. Fig. 5 compares the XRD patterns of the Na_2CO_3–Nb_2O_5 mixture in the first 40 hours of milling (Fig. 5a) with the XRD patterns of Na_2CO_3 (Fig. 5b), which was high-energy milled alone, without Nb_2O_5, with exactly the same milling conditions as the mixture. While the peaks of Na_2CO_3 when milled together with Nb_2O_5 completely disappeared after 20 hours of milling (see open triangles in Fig. 5a), this is clearly not the case even after 40 hours if Na_2CO_3 was milled alone (see Fig. 5b). The broader peaks of Na_2CO_3 after 40 hours of separate milling (Fig. 5b, 40 h) are most probably a consequence of reduced crystallite size and increase in microstrains due to creation of structural disorder. The disappearance of the original crystalline Na_2CO_3 from the mixture, suggesting amorphization, is therefore an effect triggered by the presence of Nb_2O_5 rather than a pure effect of the high-energy collisions. In relation to this mechanochemical

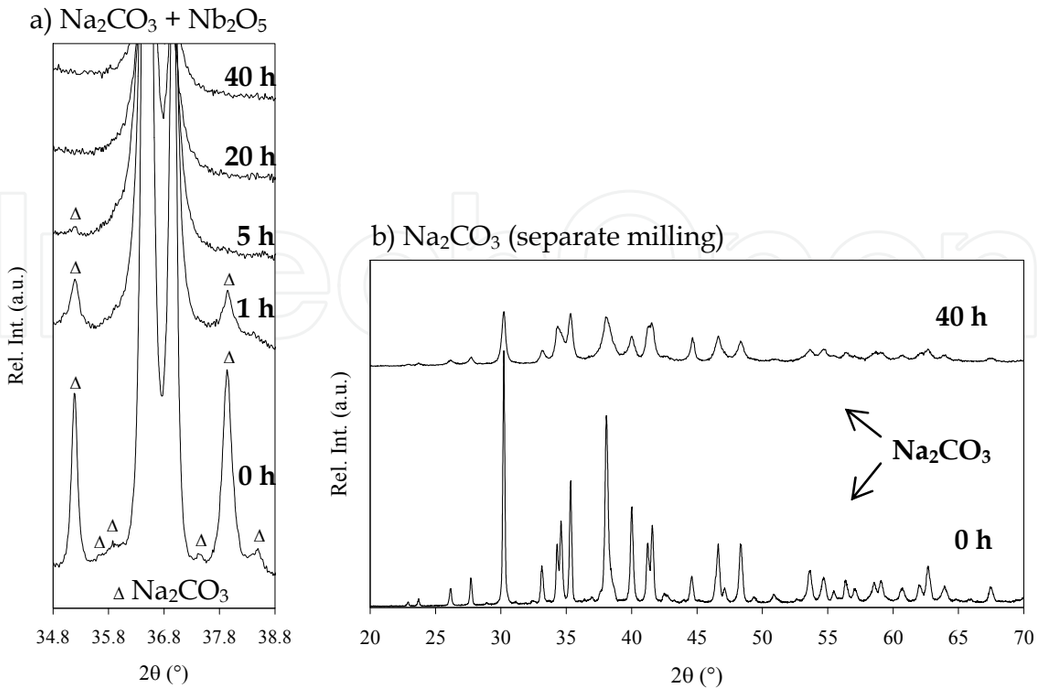

Fig. 5. XRD patterns of a) Na_2CO_3–Nb_2O_5 mixture and b) Na_2CO_3 after high-energy milling for up to 40 hours. The pattern in a) shows a narrow 2-theta region, i.e., from 34.8 to 38.8°, to highlight the changes upon milling in the peaks corresponding to Na_2CO_3. Note that all the peaks on the patterns of non-milled and 40-hours-separately-milled Na_2CO_3 in b) are indexed with monoclinic Na_2CO_3. Notation: Na_2CO_3 (Δ, PDF 19-1130); "h" denotes milling hours (from Rojac et al., 2006).

interaction between Na_2CO_3 and Nb_2O_5, a question that arises at this point is whether this interaction resulted into the carbonate decomposition. This is also relevant with respect to the nature of the amorphous phase. Obviously, further information could be obtained by following the decomposition of the carbonate during milling. This can be done using thermogravimetric (TG) analysis; the results of TG coupled with differential thermal analysis (DTA) and evolved-gas analysis (EGA) are presented in the following section.

2.2 Thermal analysis

In order to explore the origin of the reaction-induced amorphization and/or possible decomposition of Na_2CO_3 (Fig. 5) we were further focused on the initial part of milling, i.e., results are presented for the samples treated in the first 40 hours of milling.

Fig. 6 presents the thermogravimetric (TG), derivative thermogravimetric (DTG), differential thermal analysis (DTA) and evolved-gas analysis (EGA) curves of the Na_2CO_3–Nb_2O_5 powder mixture in the first 40 hours of high-energy milling. The non-milled Na_2CO_3–Nb_2O_5 mixture looses mass in several steps in a broad temperature range from 400 °C to 800 °C (Fig. 6a and b, 0 h). The total mass loss of this mixture upon annealing to 900 °C amounts to 11.7%, which agrees well with the theoretical mass loss of 11.8%, calculated according to equation 1 for the complete decomposition of Na_2CO_3 in an

equimolar mixture with Nb_2O_5. The carbonate decomposition is further confirmed by EGA, which shows a release of CO_2 in the temperature range 400–800 °C (Fig. 6d, 0 h, full line). Note also that the DTG peaks (Fig. 6b, 0 h) coincide with the EGA(CO_2) peaks (Fig. 6d, 0 h, full line), showing that the measured mass loss in this sample is indeed entirely related to the decomposition of Na_2CO_3, which is triggered by the reaction with Nb_2O_5, like represented by equation 1.

High-energy milling resulted into several changes in the thermal behaviour of the Na_2CO_3–Nb_2O_5 mixture. Firstly, by inspecting the TG curves, a mass loss appears in the milled samples in the temperature range 25–300 °C, which was not observed prior milling (Fig. 6a, compare milled samples with the non-milled). According to the DTA curves (Fig. 6c), these mass losses between room temperature and 300 °C are accompanied by endothermic heat effects, which first manifest as a sharp endothermic peak at around 100 °C (Fig. 6c, 1 h), progressively evolving with milling into a broader endothermic peak, which expands from 80 °C to 250 °C (see for example Fig. 6c, 40 h). According to EGA(H_2O), the mass losses in this low temperature range correspond to the removal of H_2O (Fig. 6d, milled samples, dashed lines). The amounts of H_2O removed from the samples milled for 0, 1, 5, 20, 40 hours, as determined from the TG curves (Fig. 6a, milled samples, 25–300 °C), are 0%, 2.5%, 4.0%, 4.8% and 5.1%, respectively. This suggests gradual adsorption of H_2O on the powder with increasing milling time; taking into account that the milling was performed in open air and also considering the hygroscopic nature of Na_2CO_3, the adsorption of H_2O is not surprising. We note that the H_2O removal from the samples milled for longer periods, i.e., 5, 20 and 40 hours, takes place at temperatures higher than 100 °C (Fig. 6d, dashed lines), which might suggest water chemisorption rather than physical adsorption.

In addition to water adsorption, high-energy milling induced considerable changes in the thermal decomposition of the carbonate. This is best seen by inspecting the DTG and EGA (CO_2) curves of the milled samples (Fig. 6b and 6d, milled samples). Firstly, it should be noted that in the temperature range between 350 °C and 500 °C the DTG peaks of the milled mixtures (Fig. 6b, milled samples) coincide with those of EGA(CO_2) (Fig. 6d, milled samples, full lines), which means that the mass loss in this temperature range is related to the CO_2 removal, i.e., to the carbonate decomposition. For the sake of discussion, we consider in the following only the EGA(CO_2) curves (Fig. 6d, full lines). In contrast to the carbonate decomposition in the non-milled mixture (Fig. 6d, 0 h, 400–800 °C), occurring in several steps and in a broad temperature range, which is characteristic for a physical mixture of Na_2CO_3 and Nb_2O_5 particles (Jenko, 2006), the mixture milled for only 1 hour releases CO_2 in a much narrower temperature range, i.e., 400–500 °C (Fig. 6d, 1 h). We attribute this effect to the smaller particle size after 1 hour of milling, which is known to decrease considerably the decomposition temperature of Na_2CO_3 in the Na_2CO_3–Nb_2O_5 mixture due to reduced diffusion paths (Jenko, 2006). In comparison with the 1-hour milled sample, upon milling for 5 hours only small changes are observed in the shape of the EGA(CO_2) peak (Fig. 6d, 5 h, 400–500 °C). After 20 hours of milling a new, weak EGA(CO_2) peak appears at 370 °C (Fig. 6d, 20 h), suggesting two-step carbonate decomposition; this peak then shifts to 400 °C upon 40 hours of milling (Fig. 6d, 40 h). Note that after 40 hours of milling the intense EGA(CO_2) peak at 420 °C becomes sharper in comparison with shorter milling times, i.e., 1, 5 and 20 hours, indicating a more uniform decomposition of the carbonate.

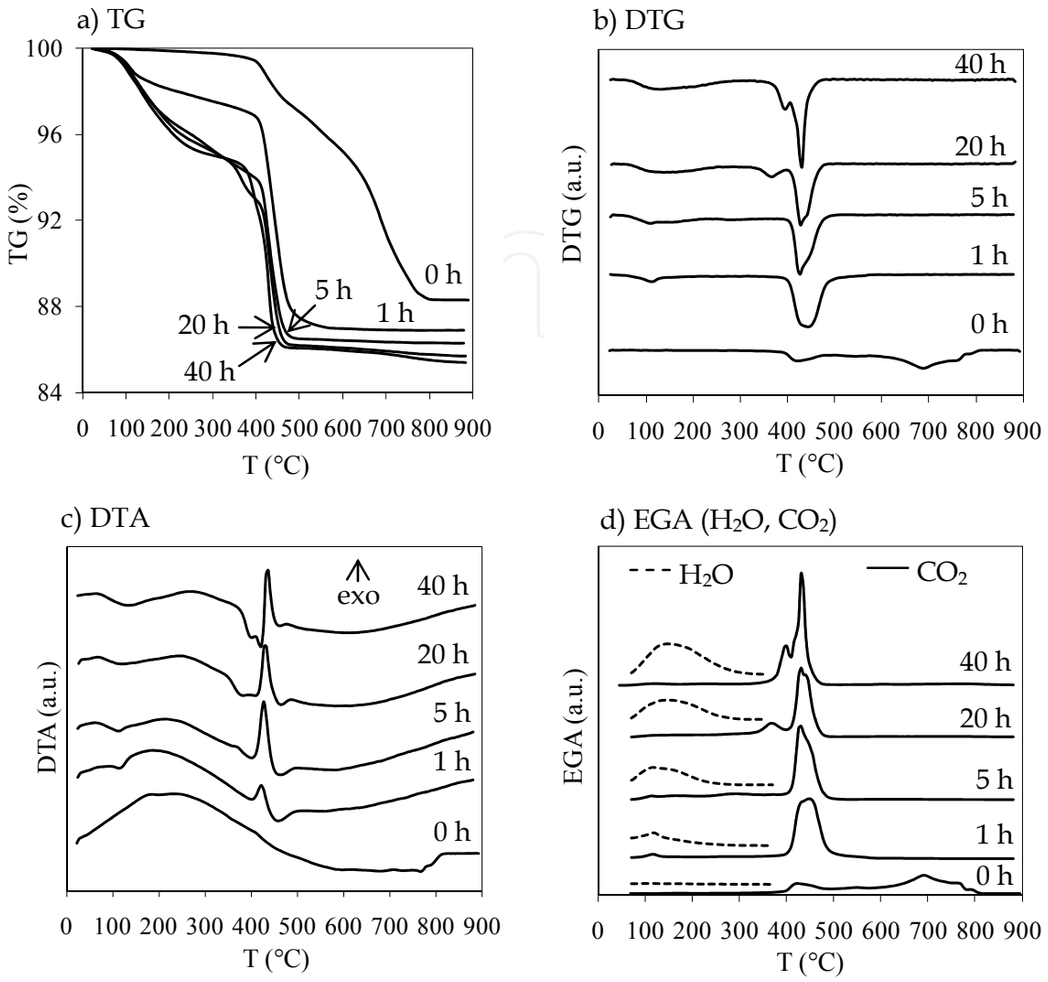

Fig. 6. a) TG, b) DTG, c) DTA and d) EGA(H_2O, CO_2) curves of the Na_2CO_3–Nb_2O_5 powder mixture after high-energy milling for 1, 5, 20 and 40 hours. The non-milled mixture is denoted as "0 h". Since the main EGA(H_2O) signal was observed in the temperature range 25–350 °C the data are plotted accordingly. "h" denotes milling hours (from Rojac et al., 2006).

According to DTA, the decomposition of the carbonate in the milled samples is accompanied by an exothermic heat effect (Fig. 6c, milled samples). This is seen from the sharp and intense exothermic peaks appearing in all the milled samples in the temperature range where the CO_2 is released, i.e., 400–500 °C (compare Fig. 6c with Fig. 6d).

To summarize, the DTA and EGA(CO_2) analyses on the milled samples (Fig. 6c and d, milled samples) suggest a rather defined carbonate decomposition occurring in a narrow temperature range, which is not typical for a physical mixture of Na_2CO_3 and Nb_2O_5 (compare 0 h with milled samples in Fig. 6c and 6d; see also Jenko, 2006); this indicates a change in the chemical state of the carbonate upon milling and formation of a new phase.

According to the mass loss related to the CO_2 release, which can be separated from the loss of H_2O by combining EGA and TG curves, we can calculate the amount of the residual

carbonate in the mixture, i.e., the amount of the carbonate that did not decompose during high-energy milling. The total CO_2 loss from the sample milled for 40 hours is 9.6%, corresponding to 85.0% of residual carbonate. Therefore, in the first 40 hours of milling, a minor amount of the carbonate decomposed, whereas the major part, according to XRD analysis (Fig. 5a), became amorphous. As mentioned in the previous section, the Na_2CO_3 amorphization is stimulated by the mechanochemical interaction with Nb_2O_5. This observation, together with the characteristic changes in the decomposition of the carbonate upon milling (Fig. 6), indicates a formation of a new carbonate compound. As a next step, it seems reasonable to explore the symmetry of the CO_3^{2-} ions, which was done using infrared spectroscopy.

2.3 Infrared spectroscopy analysis

The IR spectra of the Na_2CO_3–Nb_2O_5 mixture before and after milling for various periods are shown in Fig. 7a. The two separate graphs in Fig. 7a show two different wavenumber regions, i.e., 950–1150 cm^{-1} and 1280–1880 cm^{-1}. The spectrum of the non-milled mixture is composed of a weak band at 1775 cm^{-1} and a strong one at 1445 cm^{-1}; no bands are observed in the lower wavenumber region between 950 and 1150 cm^{-1} (Fig. 7a, 0 h). Based on the literature data, the spectrum of the non-milled mixture can be entirely indexed with

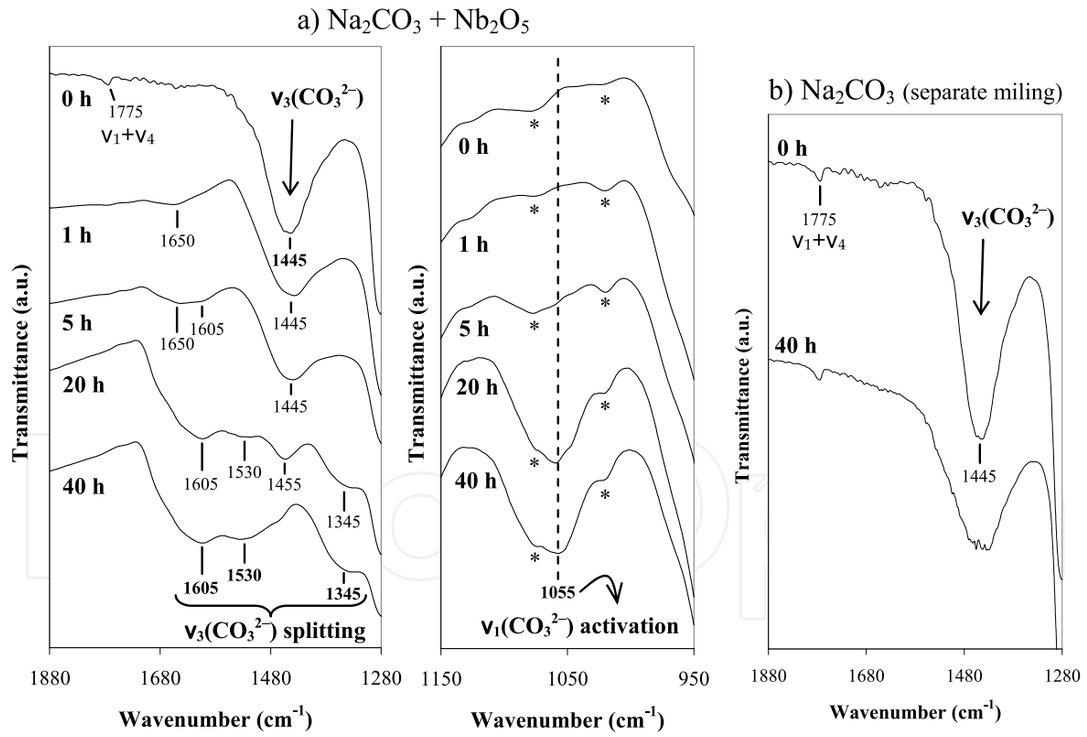

Fig. 7. FT-IR spectra of a) Na_2CO_3–Nb_2O_5 powder mixture after high-energy milling for 1, 5, 20 and 40 hours and (b) Na_2CO_3 subjected to separate high-energy milling for 40 hours. The non-milled powders are denoted as "0 h". Note that, in contrast to the Na_2CO_3–Nb_2O_5 mixture (a), no splitting of $\nu_3(CO_3^{2-})$ is observed in the case of the separately milled Na_2CO_3 (b). Notation: * Nujol, for bands assignment refer to Table 1; "h" denotes milling hours. (from Rojac et al., 2006).

vibrational bands of the CO_3^{2-} ions, present in the initial Na_2CO_3 (Harris & Salje, 1992; Gatehouse et al., 1958). This is consistent with the fact that Nb_2O_5, which is also a part of the mixture, did not show any IR bands in the two examined wavenumber regions (the IR spectrum of Nb_2O_5 is not shown).

The IR vibrations of the free CO_3^{2-} ion having D_{3h} point group symmetry are listed in Table 1. The CO_3^{2-} ion possesses two stretching and two bending vibrational modes. The symmetrical C–O stretching vibration, denoted as ν_1, is IR-inactive, while the ν_2, ν_3 and ν_4 are IR-active. According to Harris & Salje (1992), and Table 1, the strongest band of the non-milled sample at 1445 cm^{-1} (Fig. 7a, 0 h) belongs to the assymetrical C–O stretching vibration of CO_3^{2-} (ν_3), while the weak band at 1775 cm^{-1} can be assigned to the combinational band of the type $\nu_1+\nu_4$. No bands are observed in the 950–1150 cm^{-1} region (Fig. 7a, 0 h), consistent with absence of the IR-inactive ν_1 vibration. With the exception of some differences in the position, the bands of the non-milled mixture, which belong to Na_2CO_3, are consistent with vibrations characteristic for the free CO_3^{2-} ion with D_{3h} symmetry. This is in agreement with the literature data and was explained as being a consequence of the small effect of the crystal field of Na^+ ions on the symmetry of the CO_3^{2-} in the Na_2CO_3 structure. This is somewhat different, for example, in Li_2CO_3, where a stronger interaction between crystal lattice and CO_3^{2-} ions leads to lowered CO_3^{2-} symmetry and, consequently, to a more complex IR spectrum (Buijs & Schutte, 1961; Brooker & Bates, 1971).

Type of vibration	Notation	Wavenumber (cm^{-1})
C–O symmetrical stretching	ν_1 (A_1')	1063
Out-of-plane CO_3^{2-} bending	ν_2 (A_2'')	879
C–O asymmetrical stretching	ν_3 (E')	1415
In-plane CO_3^{2-} bending	ν_4 (E')	680

Table 1. Fundamental IR vibrations of carbonate (CO_3^{2-}) ion with D_{3h} symmetry. ν_2, ν_3 and ν_4 are IR-active vibrations, while ν_1 is IR-inactive (Gatehouse et al., 1958; Nakamoto, 1997).

Upon milling the Na_2CO_3–Nb_2O_5 mixture, considerable changes can be observed in the IR spectra (Fig. 7a, milled samples). After 1 hour of milling a new weak band appears at 1650 cm^{-1}. The position of this band coincides with one of the strongest HCO_3^- bands typical for alkaline hydrogencarbonates (Watters, 2005). This is in agreement with the simultaneous loss of H_2O and CO_2 upon annealing this sample (Fig. 6d, 1 h), which is characteristic for the hydrogencarbonate decomposition. Furthermore, we should not eliminate the possibility of having the in-plane bending vibration of H_2O, which also appears near 1650 cm^{-1} (Venyaminov & Prendergast, 1997).

By further milling from 1 hour to 40 hours related and simultaneous trends can be noted: i) the $\nu_3(CO_3^{2-})$ vibration shifts from 1445 cm^{-1} (Fig. 7a, 1 and 5 h) to 1455 cm^{-1} (Fig. 7a, 20 h) and decreases in intensity until it completely disappears after 40 h of milling, ii) the ν_3 vibration is gradually replaced by new absorption bands appearing at 1605, 1530 and 1345 cm^{-1} (Fig. 7a, 40 h), and iii) a new band arises during milling, located at 1055 cm^{-1}, which belongs to the symmetrical C–O stretching vibration of the CO_3^{2-} ions (ν_1) (Fig. 7a, see region 950–1150 cm^{-1}). We can conclude from these results that milling induced a splitting of ν_3 and activation of ν_1 vibrations, suggesting a change of the CO_3^{2-} symmetry from the

original D_{3h}. We shall come back to this point after examining the fundamental relation between symmetry and IR vibrations of the carbonate ion.

An extensive review on the IR spectroscopic identification of different species arising from the reactive adsorption of CO_2 on metal oxide surfaces can be found in Busca & Lorenzelli, 1982. In principle, the carbonate ion is a highly versatile ligand, which gives rise not only to simple mono- or bidentate structures, but also to a number of more complicated bidentate bridged structures. Some examples of CO_3^{2-} coordinated configurations are schematically illustrated in Fig. 8.

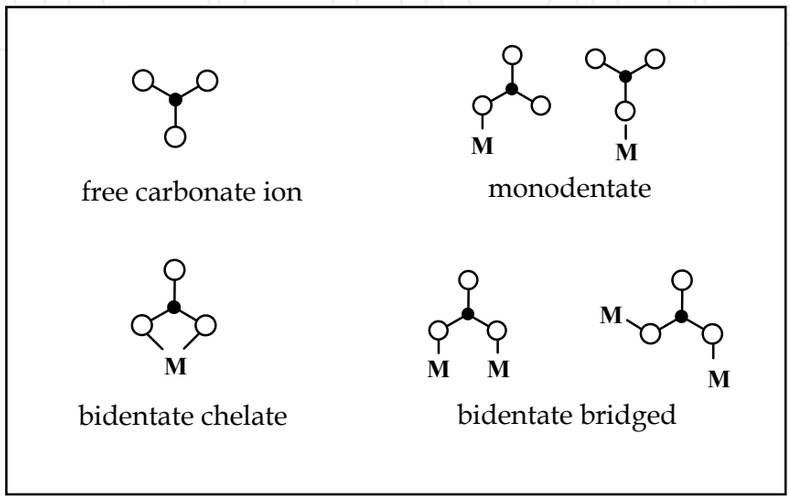

Fig. 8. Schematic view of free (non-coordinated) and various types of coordinated CO_3^{2-} ions.

When the CO_3^{2-} ion is bound, through one or more of its oxygens, to a metal cation (denoted as "M" in Fig. 8), its point group symmetry is lowered. It is well known from the literature that the lowering of the CO_3^{2-} symmetry, resulting from the coordination of the carbonate ion in a carbonato complex, causes the following changes in the IR vibrational modes of the free carbonate ion (Gatehouse et al., 1958; Hester & Grossman, 1966; Brintzinger & Hester, 1966; Goldsmith & Ross, 1967; Jolivet et al., 1980; Busca & Lorenzelli, 1982; Nakamoto, 1997):

1. Activation of IR-inactive ν_1 vibration
2. Shift of ν_2 vibration
3. Splitting of ν_3 vibration
4. Splitting of ν_4 vibration

The most characteristic of the above IR spectroscopic changes upon CO_3^{2-} coordination is the infrared activation of the ν_1, i.e., the symmetrical C–O stretching vibration. This vibration, as mentioned earlier, is IR-inactive for the free carbonate ion, but also for most alkali, alkaline-earth and heavy-metal carbonates; it appears as a weak band only in certain carbonates of the aragonite type (Gatehouse et al., 1958). To derive the relation between symmetry and IR vibrations, we shall first look at the details of the ν_1 vibration. According to the IR selection rule, which states that *the vibration is IR-active if the dipole moment is changed during vibration*, we can understand that there will be no net change in the dipole moment during symmetrical C–O stretching vibration (ν_1) of the CO_3^{2-} ion with D_{3h}

symmetry; this comes from the equivalence of the three C–O bonds, which is schematically illustrated in Fig. 9 (bottom-left quadrant). The equivalence of these three C–O bonds is lost upon coordination, so that typically the C–O bond coordinated to the metal cation becomes weaker, while the C–O bonds not involved in metal binding becomes stronger with respect to the C–O bond in the free, non-coordinated, CO_3^{2-} ion (Fig. 9, upper-right quadrant) (Fujita et al., 1962; Brintzinger & Hester, 1966). This in turn leads to lowered CO_3^{2-} symmetry, e.g., from D_{3h} to C_{2v}, and to the activation of the ν_1 vibration (Fig. 9, bottom-right quadrant). In the case of monodentate coordination, also the C_s symmetry is possible and arises when the M–O–C bond is not collinear (Fig. 9, upper-right quadrant); same IR spectroscopic changes also apply for this case (Fujita et al., 1962; Nakamoto, 1997).

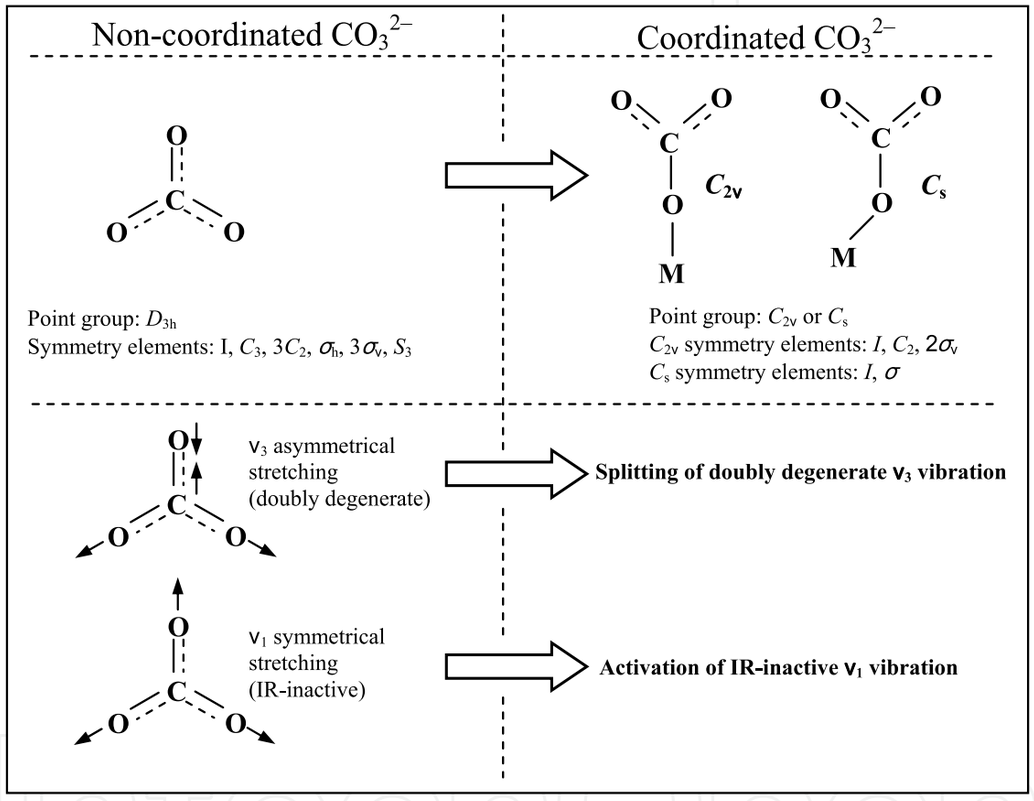

Fig. 9. Schematic representation of non-coordinated and coordinated CO_3^{2-} ion and the corresponding point group symmetry elements. The changes in the ν_1 and ν_3 IR vibrations of the CO_3^{2-} ion upon coordination are also shown. For simplicity, only monodentate coordination is presented. Notations: I – identity, C_n – n-fold axis of rotation, σ_h, σ_v – mirror planes perpendicular and parallel to the principal axis, respectively, S_n – n-fold rotation-reflection operation. The number preceding the symmetry operation symbol refers to number of such symmetry elements that the molecule possesses. For further details consult Nakamoto, 1997.

In parallel with the ν_1 activation, also the splitting of the ν_3 vibration occurs upon coordination. In the free CO_3^{2-} ion, the ν_3 vibration is doubly degenerate (Fig. 9, bottom-left quadrant). Doubly degenerate vibrations occur only in molecules possessing an axis higher than twofold, which is the case of the D_{3h} symmetry, having a three-fold rotational axis (see

Fig. 9, upper-left quadrant; C_3 – three-fold axis) (Nakamoto, 1997). The lowering of the symmetry of the carbonate ion from D_{3h} to either C_{2v} or C_s, which means loss of the equivalence of the three C–O bonds in the CO_3^{2-} and, therefore, loss of the three-fold rotational axis, leads to the separation (splitting) of the doubly degenerate vibrations (Fig. 9, bottom-right quadrant).

With respect to the changes upon coordination in the other two vibrational modes, i.e., ν_2 and ν_4, it should be noted that the splitting of the ν_4 vibration has been studied to a lesser extent in comparison with the characteristic ν_3 splitting. In addition, the shift of the ν_2 vibration upon coordination is typically small and the values for complexes do not differ greatly in comparison with those of simple carbonates (Gatehouse et al., 1958).

Coming back to our case from Fig. 7a, we can interpret the ν_3 splitting and ν_1 activation of the CO_3^{2-} vibrations during milling of the Na_2CO_3–Nb_2O_5 mixture as characteristic of lowered CO_3^{2-} symmetry, which is related to the mechanochemical formation of a carbonato complex. For comparison, we compiled in Table 2 the data of a number of carbonato complexes, with metals such as Cu and Co, provided from the literature. According to the notation of the coordinated C_{2v} symmetry, the ν_3 vibration of the D_{3h} symmetry is now split into two components, which are denoted as ν_1 and ν_4 (second and third column in Table 2); the activated ν_1 vibration becomes ν_2 (fourth column in Table 2). The regions in which the carbonato complex absorption bands appear are 1623-1500 cm^{-1}, 1362-1265 cm^{-1} (ν_3 splitting) and 1080-1026 cm^{-1} (ν_1 activation) (Table 2). By comparing these data with the our case, we can observe that the ν_3 split bands at 1605, 1530 and 1345 cm^{-1}, and the ν_1 activated band at 1055 cm^{-1} from Fig. 7a (40 h) fall entirely within the wavenumber regions of carbonato complexes from Table 2.

Carbonato complex	**$\nu_4(B_2)$ (cm^{-1})**	**$\nu_1(A_1)$ (cm^{-1})**	**$\nu_2(A_1)$ (cm^{-1})**
$Na_2Cu(CO_3)_2$	1500	1362	1058
$Na_2Cu(CO_3)_2{\cdot}3H_2O$	1529	1326	1066, 1050
$K_3Co(CO_3)_3{\cdot}3H_2O$	1527	1330	1080, 1037
$KCo(NH_3)_2(CO_3)_2$	1623, 1597	1265	1026
$Co(NH_3)_6Co(CO_3)_3$	1523	1285	1073, 1031
$Co(NH_3)_4CO_3Cl$	1593	1265	1030
$Co(NH_3)_4CO_3ClO_4$	1602	1284	not reported

Table 2. Some copper and cobalt carbonato complexes and the corresponding IR absorption bands related to CO_3^{2-} vibrations. ν_1, ν_2 and ν_4 correspond to vibrations of CO_3^{2-} in the C_{2v} symmetry notation; according to this notation, the doubly degenerate ν_3 vibration of the free CO_3^{2-} ion, which splits into two components, is denoted as ν_1 and ν_4, whereas the activated ν_1 vibration is denoted as ν_2 (data compiled from Gatehouse et al., 1958; Fujita et al., 1962; Jolivet et al., 1982; Healy & White, 1972).

It is important to note that, in contrast to the Na_2CO_3–Nb_2O_5 mixture, the ν_3 vibration did not split when Na_2CO_3 was milled alone, i.e., without Nb_2O_5. This is seen in Fig. 7b, which shows the IR spectra of Na_2CO_3 before and after separate milling. Except for the reduced intensity, which might be related to the decreased crystallite size and structural disordering

induced by milling, the ν_3 band at 1445 cm^{-1} is still present after 40 hours of separate milling. We emphasize that for this separate Na_2CO_3 milling the same milling conditions and same milling time, i.e., 40 hours, were applied as for the Na_2CO_3–Nb_2O_5 mixture. Therefore, the lowering of the CO_3^{2-} symmetry and the corresponding coordination of the CO_3^{2-} ions can only be explained by the presence of Nb_2O_5 or, in other words, by the participation of Nb^{5+} as central cation.

The mechanochemical formation of the carbonato complex is further supported by XRD analysis. By comparing XRD and IR data, we find that the ν_3 splitting and ν_1 activation, which took place progressively from 5 to 40 hours of milling (Fig. 7a), coincide with the amorphization of Na_2CO_3 (Fig. 5a). For example, after 20 hours of milling, when the split ν_3 bands are resolved for the first time and intense ν_1 band appeared (Fig. 7a, 20 h), the XRD peaks of Na_2CO_3 could not be detected anymore (Fig. 5a, 20 h). From this comparison we can conclude that the amorphization of Na_2CO_3 is closely related to the formation of the complex. The conclusion seems reasonable if we consider that the formation of the complex requires a reconstruction, i.e., coordination, of the CO_3^{2-} ions; such reconstruction can eventually ruin the original Na_2CO_3 structure over the long range, make it undetectable to X-ray diffraction. The relation between amorphization and coordination is further supported by the fact that neither the amorphization of Na_2CO_3 nor the ν_3 splitting were observed during separate milling of Na_2CO_3 (see Fig. 5b and Fig. 7b).

We finally note that after 40 hours of milling the powder mixture contains 81% of XRD-amorphous phase (inset of Fig. 4b). According to this large amount and based on the fact that we did not detect any new crystalline phase during 40 hours of milling we can conclude that the carbonato complex is amorphous or eventually nanocrystalline to an extent that is undetectable with X-ray diffraction methods. This example illustrates that enriched information on a local structural scale can only be achieved by appropriate selection of analytical tools. The amorphous carbonato complex has recently been confirmed using Raman and nuclear magnetic resonance (NMR) spectroscopies (Rojac et al., to be published).

Another important aspect to discuss is the possible role of water on of the formation of the complex. Jolivet et al. (1982) emphasized the influence of the water molecules on the ν_3 splitting, which can be significant, depending on whether they can interact via hydrogen bonding with the carbonate group. This was demonstrated through various examples of lanthanide carbonates, where the hydrated forms showed different ν_3 splitting with respect to their dehydrated analogues. As an example, the hydrated form of the $Na_2Cu(CO_3)_2$ complex, that is $Na_2Cu(CO_3)_2{\cdot}3H_2O$, showed larger $\Delta\nu_3$ splitting, i.e., 203 cm^{-1}, in comparison with its dehydrated form, i.e., 138 cm^{-1} (see also Table 2, first two examples).

In our case, the possible influence of water molecules on the carbonate ion should be considered. In fact, we showed in section 2.2 (Fig. 6) that an amount of water was introduced in the sample from the air during the milling. Therefore, we have to examine more carefully the possible influence of water adsorption on the ν_3 splitting. This was done by quenching the 40-hours-treated sample in air from different temperatures so that controlled amounts of water were released; the quenched samples were then analyzed using IR spectroscopy. The IR spectra together with the TG and EGA curves are shown in Fig. 10. The mass losses after quenching at 100 °C, 170 °C and 300 °C were 0.8 %, 3.1 % and 5.0 %,

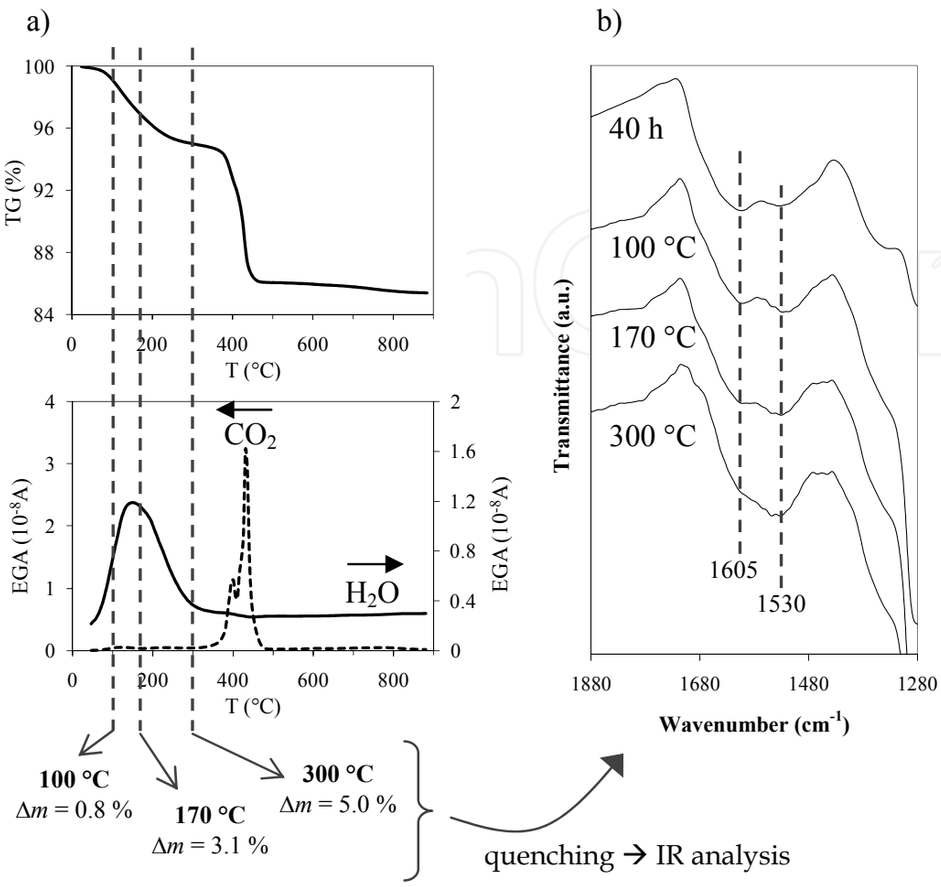

Fig. 10. a) TG and EGA(H_2O,CO_2) curves of the 40-hours high-energy milled Na_2CO_3–Nb_2O_5 powder mixture. The dashed lines on the graphs represent the temperatures at which the 40-hours milled sample was air-quenched. b) FT-IR spectra of the 40-hours high-energy milled Na_2CO_3–Nb_2O_5 powder mixture air-quenched from various temperatures (from Rojac et al., 2006).

respectively. According to EGA, these mass losses correspond entirely to the removal of water (Fig. 10a, see dashed lines). From Fig. 10b we can see that with increasing amount of released H_2O the band at 1605 cm^{-1} gradually decreases at the expense of the band at 1530 cm^{-1}. Note that the intensity of the band at 1345 cm^{-1} decreases, too. The results confirm the influence of H_2O on the splitting of the ν_3 vibration.

There are some cases of carbonato complexes, as pointed out by Jolivet et al. (1982), in which water molecules can even modify the coordination state of the carbonate ion. This is also the case of the $Na_2Cu(CO_3)_2{\cdot}3H_2O$ complex, which contains both bidentate chelate and bridged carbonate ions, whereas its dehydrated form is exclusively a bridged structured (see also Fig. 8). Concerning our carbonato complex, it would be interesting to get more information about the actual influence of H_2O on the CO_3^{2-} coordination. Since apparently the H_2O has an active role in the mechanochemical formation of the complex, namely, it affects the ν_3 splitting, and taking into account that this complex represents an intermediate phase from which the $NaNbO_3$ is formed, it would also be interesting to find out whether milling in

humid-free conditions will affect the formation of the niobate. These questions will be left for further investigations.

3. Mechanochemical reaction rate in Na_2CO_3–M_2O_5 (M = V, Nb, Ta) powder mixtures

3.1 Quantitative X-ray diffraction, infrared spectroscopy and thermogravimetric analysis

In-depth study of reaction mechanism limited to one system is often insufficient if fundamental characteristics governing certain type of mechanochemical reaction are to be determined. Following the results from the previous section, in which we identified an amorphous carbonato complex as a transitional stage of the reaction between Na_2CO_3 and Nb_2O_5, it is the next step to find out i) whether this mechanism is general for mechanochemical reactions involving CO_3^{2-} ions and ii) which parameters control the decomposition of the carbonato complex. The latter is particularly important as the decomposition of the complex is a necessary step for the formation of the final binary oxide.

In order to study systematically the mechanochemical interaction between CO_3^{2-} ions and various metal cations, which could possibly lead to the formation of the carbonato complex, we explored the reactions involving Na_2CO_3, as one reaction counterpart, and various 5th group transition-metal oxides, including V_2O_5, Nb_2O_5 and Ta_2O_5. The aim of the study was to determine the influence of the transition-metal oxide on i) the mechanochemical decomposition of Na_2CO_3 and ii) the rate of formation of the target binary oxides, i.e., $NaVO_3$, $NaTaO_3$ and $NaNbO_3$.

The mechanochemical formation of $NaMO_3$ (M = V, Nb, Ta) from respective Na_2CO_3–M_2O_5 (M = V, Nb, Ta) mixtures was followed by quantitative X-ray diffraction phase analysis using Rietveld refinement method. The fractions of $NaMO_3$ (M = V, Nb, Ta) as a function of milling time are shown in Fig. 11. The rate of formation of the final oxides follows the order $NaVO_3$>$NaTaO_3$>$NaNbO_3$. Note that the vanadate was formed within 4 hours, while the

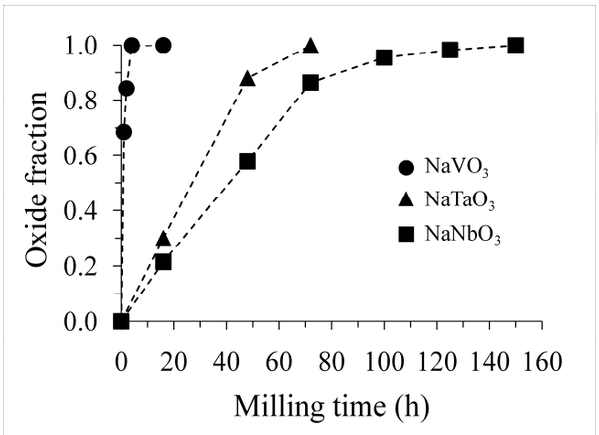

Fig. 11. Fraction of $NaMO_3$ (M = V, Nb, Ta), determined by Rietveld refinement analysis, as a function of milling time. The lines are drawn as a guide for the eye (from Rojac et al., 2011).

tantalate and niobate required much longer milling times to be the only crystalline phase detected in the mixtures, i.e., 72 and 150 hours, respectively. The results show that the type of the transition-metal oxide plays an important role in the formation kinetics of $NaMO_3$ (M = V, Nb, Ta).

In order to verify whether the amorphous carbonato complex appears as a transitional phase in the three examined reactions, we performed an IR spectroscopy analysis. The results are presented in Fig. 12. In all the systems, a common trend, characteristic for the lowering of the CO_3^{2-} symmetry, is observed during milling: i) the $\nu_3(CO_3^{2-})$ vibration shifts gradually to higher wavenumbers and decreases in intensity until it disappears after certain milling time, ii) the ν_3 vibration is replaced by new bands in the region 1650–1250 cm^{-1}, showing ν_3 splitting (see 4 h, 72 h, 150 h in Fig. 12 a, b and c, respectively) and iii) the ν_1 vibration is activated. Note that the ν_1 activation in the case of the Na_2CO_3–V_2O_5 mixture could not be ascertained due to overlapping with the band at 1025 cm^{-1}, related to the stretching vibration of the double vanadyl V=O bonds of V_2O_5 (Fig. 12a). According to the relation between symmetry and IR vibrational spectroscopy of the CO_3^{2-} ion, described in detail in the previous section, the formation of the carbonato complex is confirmed in all the examined systems.

We note that the milling conditions for the mechanochemical synthesis of $NaNbO_3$ presented in the previous section were different from the ones that we applied for the study presented here. This is seen from the different kinetics of the formation of $NaNbO_3$, i.e., by comparing the timescale of the $NaNbO_3$ fraction-versus-time curves from Fig. 11 (closed rectangular) and Fig. 4b (open circles). Therefore, the mechanism of the mechanochemical interaction between Na_2CO_3 and Nb_2O_5, in terms of the transitional carbonato complex, is qualitatively unaffected by the milling intensity.

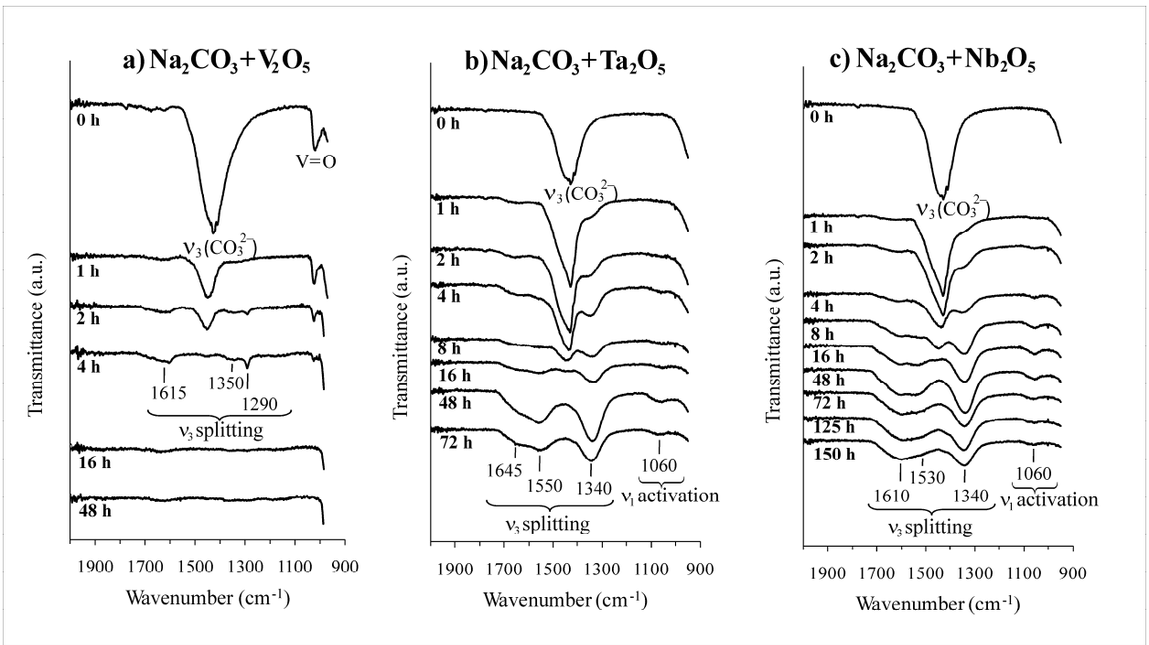

Fig. 12. FT-IR spectra of Na_2CO_3–M_2O_5 (M = V, Nb, Ta) powder mixtures after different milling times (from Rojac et al., 2011).

The results from Fig. 12 suggest a general reaction mechanism in mixtures involving CO_3^{2-} ions; in fact, in addition to the systems presented in this chapter, the carbonato complex was identified in a number of other alkaline-carbonate–transition-metal oxide mixtures, including the following:

- Li_2CO_3–Nb_2O_5 (unpublished work)
- K_2CO_3–Nb_2O_5 (Rojac et al., 2009)
- Rb_2CO_3–Nb_2O_5 (unpublished work)
- K_2CO_3–Ta_2O_5 (Glinsek et al., 2011)
- Na_2CO_3–K_2CO_3–Nb_2O_5 (unpublished work)
- Na_2CO_3–K_2CO_3–Nb_2O_5–Ta_2O_5 (Rojac et al., 2010)
- Na_2CO_3–K_2CO_3–$Li_2C_2O_4$–Nb_2O_5–Ta_2O_5 (Rojac et al., 2010)

A closer inspection of Fig. 12 reveals several differences between the three reaction systems. First of all, the degree of the ν_3 splitting is different depending on the metal cation, i.e., V^{5+}, Nb^{5+} or Ta^{5+}, to which the CO_3^{2-} coordinate. The maximum splitting of ν_3 from the spectra of the Na_2CO_3–M_2O_5 (M = V, Ta, Nb) mixtures after 4, 72 and 150 hours of milling, respectively (Fig. 12), is collected in Table 3. The maximum $\Delta\nu_3$ splitting is largest in the case of V_2O_5 (325 cm^{-1}), followed by Ta_2O_5 (305 cm^{-1}) and Nb_2O_5 (270 cm^{-1}).

Mixture	Max $\Delta\nu_3$ splitting (cm^{-1})
Na_2CO_3–V_2O_5	325
Na_2CO_3–Ta_2O_5	305
Na_2CO_3–Nb_2O_5	270

Table 3. Maximum splitting of $\nu_3(CO_3^{2-})$ vibration in Na_2CO_3–M_2O_5 (M = V, Nb, Ta) powder mixtures (from Rojac et al., 2011).

Nakamoto et al. (1957) were the first to propose the degree of ν_3 splitting ($\Delta\nu_3$) as a criterion to distinguish between mono- and bidentate coordination in carbonato complexes. Their results showed that some bidentate cobalt carbonato complexes have $\Delta\nu_3$ splitting of about 300 cm^{-1}, while monodentate complexes of analogous chemical composition exhibit about 80 cm^{-1} of $\Delta\nu_3$. Calculations based on models of XO_3 (X = C, N) groups coordinated to a metal cation confirmed the larger splitting in the case of bidentate coordination, as compared to the monodentate coordination (Britzinger & Hester, 1966; Hester & Grossman, 1966). A general relationship between the type of coordination and $\Delta\nu_3$ splitting, which we updated according to the critical review by Busca & Lorenzelli (1982), is shown schematically in Fig. 13a. While monodentate configurations show splitting of around 100 cm^{-1} or lower, larger $\Delta\nu_3$ splitting can be expected for bidentate chelate and bidentate bridged coordinations.

In addition to the type of coordination, other factors influence the degree of the ν_3 splitting. As explained in the previous section, the coordination of the CO_3^{2-} ion causes a rearrangement of the C–O bonds, i.e., the C–O bond coordinated to the metal cation is typically weakened, while the others, non-coordinated, are strengthened. Calculations showed that, for a given type of coordination, this CO_3^{2-} polarization is more pronounced if the polarizing power of the central cation is high as it can attracts electrons more strongly (Britzinger & Hester, 1966). The $\Delta\nu_3$ splitting, which reflects the CO_3^{2-} polarization, should

therefore depend on the polarizing power of the central cation. This was indeed confirmed experimentally by Jolivet et al. (1982), which identified a linear increase of $\Delta\nu_3$ splitting with the polarizing power of the central cation for numerous carbonato complexes having the same bidentate coordination (Fig. 13b). For those cases, the polarizing power of the cation was assumed to be proportional to e/r^2, where e and r are cation charge and radius, respectively. Therefore, the $\Delta\nu_3$ splitting criterion for distinguishing between different types of coordination (Fig. 13a) should only be applied if the polarizing power of the cation is taken into account (Fig. 13b). As pointed out by Busca & Lorenzelli (1982), low values of $\Delta\nu_3$ splitting, e.g., ~100 cm^{-1}, do not unequivocally indicate the presence of monodentate structure, particularly in cases of metals having low polarizing power (se also Fig. 13b).

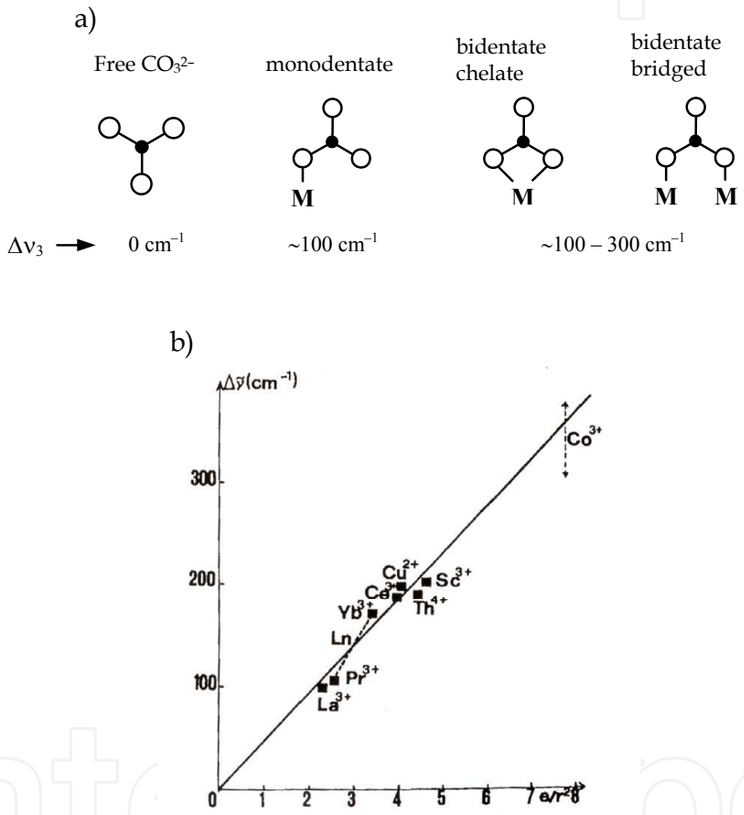

Fig. 13. a) Schematic view of the influence of the type of coordination on splitting of $\nu_3(CO_3^{2-})$ vibration (from Busca & Lorenzelli, 1982) and b) correlation between splitting of $\nu_3(CO_3^{2-})$ vibration and polarizing power (e/r^2) of the central cation for bidentate carbonato complexes. "e" and "r" denote cation charge and radius, respectively (from Jolivet et al., 1982).

By comparing with the literature data and considering the relationship shown in Fig. 13a, the maximum $\Delta\nu_3$ splitting in the three mixtures from Table 3, being larger than 100 cm^{-1}, might suggest bidentate chelate and/or bridged coordination. The increasing $\Delta\nu_3$ from the system with niobium, having the smallest $\Delta\nu_3$ of 270 cm^{-1}, to that with vanadium, with the largest $\Delta\nu_3$ of 325 cm^{-1} (Table 3), correlates with the increasing cation acidity, appearing in

the order $Nb^{5+}<Ta^{5+}<V^{5+}$ (see Xz/CN values in Table 5 and refer to the next section for details). Since it is generally accepted that the acidity scales with the cation charge density, i.e., *e*/*r* (Avvakumov et al., 2001), our correlation, in principle, agrees with the one of Jolivet et al. (1982) from Fig. 13b. However, even if a correlation exists, it should be interpreted carefully since in addition to the polarizing ability of the central cation, we should not neglect other influences on the $\Delta\nu_3$ splitting, such as, for example, incorporation of water molecules, as demonstrated in previous section (Fig. 10), which might differ between the three examined systems.

In addition to the ν_3 splitting, another difference between the three reactions that should be noted is the much faster formation of the complex in the case of V^{5+} as central cation in comparison with Nb^{5+} and Ta^{5+} (Fig. 12). This can be seen by comparing the characteristic ν_3 splitting among the three systems taking into consideration the point of the transition of the original ν_3 vibration into split bands as a criterion for the CO_3^{2-} coordination (Fig. 12). Whereas in the case of V_2O_5 the ν_3 vibration almost completely disappeared after 4 hours of milling, giving rise to split bands (Fig. 12a), at least 16 hours were needed in the case of Nb_2O_5 and Ta_2O_5 (Fig. 12b and c). This is in agreement with the kinetics of $NaMO_3$ formation (M = V, Nb, Ta), shown in Fig. 11.

In contrast to the Na_2CO_3–Ta_2O_5 and Na_2CO_3–Nb_2O_5 systems, where the IR absorption bands of the carbonato complex are still clearly resolved after 72 and 150 hours of milling (Fig. 12b and c), these bands completely disappeared after only 16 h of milling in the case of the Na_2CO_3–V_2O_5 mixture (Fig. 12a). A reasonable explanation for the absence of the IR bands related to the complex is its decomposition. If this is the case, it suggests that the transition-metal oxide plays a role in the decomposition of the carbonato complex.

We can compare quantitatively the carbonate decomposition in the three studied systems by using thermogravimetric analysis. Similarly like explained in the previous section, by separating the mass loss related to the H_2O release from the one that is due to the CO_2 release, we can estimate the amount of the residual carbonate in the powder mixtures. The results of this analysis are shown in Fig. 14. As expected, in all the mixtures the carbonate fraction decreases with increasing milling time; this is associated with the mechanochemically driven carbonate decomposition. We can summarize the reaction as follows: after being formed (Fig. 12), the carbonato complex decomposes (Fig. 14), leading to the formation of the final $NaMO_3$ oxides (Fig. 11). Note that, in terms of the reaction timescale, these three stages are not clearly separated, instead, they are overlapped.

The results of TG analysis (Fig. 14) reveal a substantial difference in the decomposition rate of the carbonate between the three systems: the fastest is in the case of V_2O_5, followed by Ta_2O_5 and Nb_2O_5. Note also that the carbonate fraction reaches a plateau after prolonged milling, which we denote here as the "steady-state" milling condition. The amount of the carbonate in this "steady-state" condition depends strongly on the type of the transition-metal oxides participating in the reaction. Whereas the carbonato complex decomposed nearly completely in the case of vanadium, i.e., only 0.5% of residual carbonate was determined in the "steady-state" milling condition, 29% and 39% remained in the mixture in the case of Ta and Nb, respectively (Fig. 14 and Table 4). This is in agreement with the IR spectra from Fig 12, i.e., in contrast to the cases with Nb and Ta, no IR bands related to the carbonato complex are observed after prolonged milling of the Na_2CO_3–V_2O_5 mixture (Fig.

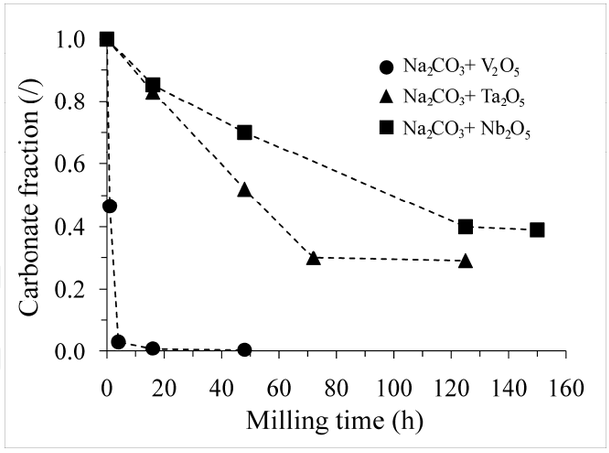

Fig. 14. Fraction of carbonate, determined by TG analysis, as a function of milling time in Na_2CO_3–M_2O_5 (M = V, Nb, Ta) powder mixtures. The lines are drawn as a guide for the eye (from Rojac et al., 2011).

Mixture	Carbonate fraction (%)
Na_2CO_3–V_2O_5	0.5
Na_2CO_3–Ta_2O_5	29
Na_2CO_3–Nb_2O_5	39

Table 4. Fraction of residual carbonate in Na_2CO_3–M_2O_5 (M = V, Nb, Ta) powder mixtures in the "steady-state" milling conditions (see carbonate fraction after prolonged milling in Fig. 14) (from Rojac et al., 2011).

12a, see 16 and 48 hours). Finally, it is important to stress that the complex is amorphous and could not be analyzed using Rietveld analysis (Fig. 11); instead, we were able to follow its formation and decomposition using IR and TG analyses, respectively (Fig. 12 and 14).

From the presented results we can infer that a common mechanism, characterized by the formation of an intermediate amorphous carbonato complex, link the reactions between Na_2CO_3 and M_2O_5 (M = V, Nb, Ta); however, considerable differences exist in the rate of the formation and decomposition of this carbonato complex and, consequently, in the crystallization of the final binary compounds. The sequence of the rates of these reactions, i.e., Na_2CO_3–V_2O_5>Na_2CO_3–Ta_2O_5>Na_2CO_3–Nb_2O_5, can be interpreted by considering the acid-base properties of the reagents involved.

3.2 Acid-base mechanochemical reaction mechanism

In their extensive work on the mechanochemical reactions involving hydroxide–oxide mixtures, Senna and co-workers (Liao & Senna, 1992, 1993; Watanabe et al., 1995b, 1996, Avvakumov et al., 2001) showed that the mechanism in these mixtures is governed by an acid-base reaction between different hydroxyl groups on the solid surface. The driving force for these reactions is the acid-base potential, i.e., the difference in the acid-base properties between an acidic and basic surface –OH group, which is determined by the type of metal on which it is bound, and therefore, on the strength of the M–OH bond (M denotes the

metal). For example, in the case of the $M(OH)_2$–SiO_2 (M = Ca, Mg) mixtures, they showed experimentally that a larger acid-base potential between $Ca(OH)_2$ and SiO_2 brought a faster mechanochemical interaction (Liao & Senna, 1993).

The acid-base reaction mechanism is not confined to the hydroxyl groups only. Thermodynamic calculations showed that a correlation exists between the Gibbs free energies of a variety of reactions between oxide compounds and the acid-base potential between the participating oxide reagents for two-component systems: the larger the potential, the more negative the value of the Gibbs energy and, thus, the faster and more complete the reaction (Avvakumov et al., 2001).

In order to fully consider the acid-base properties of oxide compounds, one should take into account that the acidity of a cation, incorporated into a certain oxide compound, depends on the oxidation state and the coordination number. For example, when the oxidation degree of the manganese ion increases by unity, the acidity increases by 2–3 times; same trend is observed when the coordination number of Si^{4+} decreases from 6 to 4. For correct comparisons, the influence of these parameters on the acid-base properties of cations should be taken into account. This can be done by introducing the electronegativity of a cation, divided by the coordination number, which defines the cation-ligand force per one bond in a coordination polyhedron; the larger the force, the larger the acidity of the cation, i.e., the stronger is the ability to attract electron pairs forming covalent bonds (Avvakumov et al., 2001).

To address the acid-base properties of the transition-metal cations, we adopted the electronegativity scale for cations derived by Zhang (1982). Table 5 shows the electronegativities Xz for V^{5+}, Ta^{5+} and Nb^{5+}. The ratio Xz/CN, where CN refers to the coordination number of the cation, taken as being indicative of the acidity of the cations in their respective oxides, is the highest for V^{5+}, followed by Ta^{5+} and Nb^{5+}.

Cation	Xz	Xz/CN
V^{5+}	2.02	0.40
Ta^{5+}	1.88	0.29
Nb^{5+}	1.77	0.27

Table 5. Electronegativity values Xz and Xz/CN ratios for V^{5+}, Nb^{5+} and Ta^{5+}. Xz and CN denote cation electronegativity defined by Zhang and coordination number, respectively. The Xz/CN ratio is taken as a parameter proportional to cation acidity (from Rojac et al., 2011).

The order of the cation acidity, i.e., $V^{5+}>Ta^{5+}>Nb^{5+}$ (Table 5) correlates with our experimental results; in fact, the reaction rate follows the same order, i.e., Na_2CO_3–V_2O_5>Na_2CO_3–Ta_2O_5>Na_2CO_3–Nb_2O_5 (see Fig. 11). This means that the higher is the acidity of the cation involved, the faster is the reaction, including the formation and decomposition of the carbonato complex (Fig. 12 and 14), and the crystallization of the final oxides (Fig. 11). The agreement between the reaction rate sequence and the cation acidity or acid-base potential, where Na_2CO_3 is taken as basic and transition-metal oxides as acidic compound, suggests that the mechanochemical reactions studied here suit the concept of an acid-base interaction mechanism. Similar correlations between the acid-base properties and the mechanochemical reaction rate can also be found in other systems comprising CaO, as one reagent, and Al_2O_3, SiO_2, TiO_2, V_2O_5 or WO_3, as the other reagent (Avvakumov et al. 1994).

We showed in the previous section that after reaching a specific milling time ("steady-state" milling condition), the fraction of the residual carbonate did not change any longer if further milling was applied (Fig. 14). These carbonate fractions correlate with the acidity of the cations as well (compare Table 4 with Table 5). Note that the small carbonate fraction in the Na_2CO_3–V_2O_5 system, i.e., 0.5 % (Table 4), is consistent with the much larger acidity of V^{5+} as compared to Ta^{5+} or Nb^{5+} (see XZ/CN values in Table 5). The results seem reasonable considering the relation that was found between the acid-base potential and the reaction Gibbs free energy; however, insufficient thermodynamic data for the systems presented here prevent us from making further steps in this direction. We note that these results carry practical consequences, i.e., they suggest that attempting to eliminate the carbonate from a mixture, characterized by a low acid-base potential, by intensifying the milling might not be successful. In fact, the residual carbonate fraction seems to be dependent on the acid-base potential, which is a characteristic of a system, rather than on the milling conditions (Rojac et al., 2008b).

Even if the rate of the three examined reactions apparently agrees with the acid-base reaction concept, we shall not neglect other parameters that could influence the course of the reaction, such as, e.g., adsorption of H_2O during milling, which might differ from one system to another. In order to directly verify this possibility, we plot in Fig. 15 the reaction rate constant versus Xz/CN. The reaction rate constant was obtained by fitting the curves from Fig. 11 with a kinetic model proposed for mechanochemical transformations in binary mixtures (Cocco et al., 2000). A linear relationship would be expected if the reaction rate will be largely dominated by the cation acidity. While the sequence of the reaction rate constants, i.e., V>Ta>Nb, agrees with the acid-base reaction mechanism, the non-linear relationship between the rate constant and Xz/CN from Fig. 15 suggests that, in addition to the cation acidity, probably other factors influence the reaction rate. The origin of these additional influences will be left open for further studies.

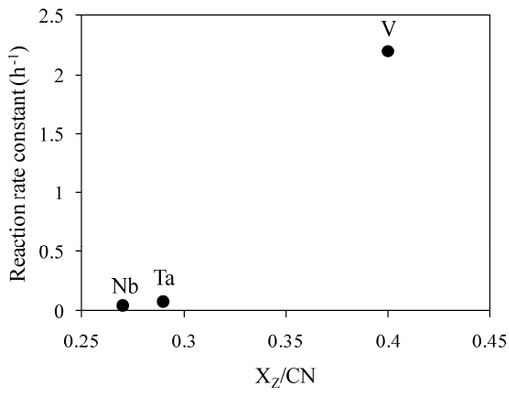

Fig. 15. Reaction rate constant versus X_Z/CN for the reactions between Na_2CO_3 and M_2O_5 (M = V, Nb, Ta) (from Rojac et al., 2011).

4. Conclusions

A systematic study of the reaction mechanism during high-energy milling of a Na_2CO_3–Nb_2O_5 mixture, presented in the first part of the chapter, revealed that the synthesis of $NaNbO_3$ takes place through an intermediate amorphous stage. Quantitative phase analysis using XRD diffraction and Rietveld refinement method showed indeed a large amount of

the amorphous phase, i.e., of up of 91%, formed in the initial part of the reaction. The amount of this amorphous phase then decreased by subsequent milling, leading to the crystallization of the final $NaNbO_3$. Only limited information, including mainly the identification of the transitional nature of the amorphous phase, was obtained using quantitative XRD phase analysis.

The decomposition of the carbonate in the Na_2CO_3–Nb_2O_5 mixtures was analyzed using TG analysis coupled with DTA and EGA. By following the carbonate decomposition upon annealing the mixtures milled for various periods we were able to infer about the changes occurring in the carbonate during high-energy milling. Characteristic changes in the carbonate decomposition upon increasing the milling time suggested a formation of an intermediate carbonate compound with rather defined decomposition temperature occurring in a narrow temperature range; such decomposition was found to be atypical for physical mixtures of Na_2CO_3 and Nb_2O_5 powders.

A more accurate identification of the amorphous phase was made possible using IR spectroscopy analysis. Characteristic IR vibrational changes during milling, including splitting of ν_3 and activation of ν_1 C–O stretching vibrations of the CO_3^{2-} ion, suggested lowered CO_3^{2-} symmetry, which was interpreted as being a consequence of CO_3^{2-} coordination and formation of an amorphous carbonato complex.

Expanding the study of the Na_2CO_3–Nb_2O_5 to other systems, we showed in the second part of the chapter that the mechanism involving the transitional amorphous carbonato complex is common for several alkaline-carbonate–transition-metal oxide mixtures, including Na_2CO_3–M_2O_5 (M = V, Nb, Ta). The sequence of the reaction rate in these three systems, including the formation of the complex, its decomposition and crystallization of the final $NaMO_3$ (M = V, Nb, Ta), was interpreted by considering the acid-base reaction mechanism. The largest the acid-base potential, i.e., the difference between acidic and basic properties of the reagents involved, the faster the mechanochemical reaction.

5. Acknowledgments

The work was supported by the Slovenian Research Agency within the framework of the research program "Electronic Ceramics, Nano, 2D and 3D Structures" (P2-0105) and postdoctoral project "Mechanochemical Synthesis of Complex Ceramic Oxides" (Z2-1195). For the financial support, additional acknowledgements go to Network of Excellence MIND, COST Actions 528 and 539, and bilateral project PROTEUS BI-FR/03-001. For valuable discussions on the topic we thank Barbara Malič and Janez Holc. For the help with various analytical methods, Jana Cilenšek, Bojan Kozlevčar, Edi Krajnc, Anton Meden, Andreja Benčan, Goran Dražič and Bojan Budič are sincerely acknowledged. A special thank is given for the help in the laboratory to Sebastjan Glinšek, Mojca Loncnar, Tanja Urh, Živa Trtnik and Silvo Drnovšek. Collaborations from abroad include Olivier Masson and René Guinebretière from SPCTS, University of Limoges, France, and Bozena Hilczer and Maria Polomska from the Institute of Molecular Physics, Polish Academy of Sciences, Poznan, Poland.

6. References

Avvakumov, E. G.; Devyatkina, E. T. & Kosova, N. V. (1994). Mechanochamical Reactions of Hydrated Oxides. *Journal of Solid State Chemistry*, Vol.113, No.2, pp. 379–383.

Avvakumov, E.; Senna, M. & Kosova, N. (2001). *Soft Mechanochemical Synthesis,* Kluwer Academic Publisher, Boston, USA.

Boldyrev, B. B. & Tkacova, K. (2000). Mechanochemistry of Solids : Past, Present, and Prospects. *Journal of Materials Synthesis and Processing*, Vol.8, No.3-4, pp. 121–132.

Brintzinger, H. & Hester, R. E. (1966). Vibrational Analysis of Some Oxyanion-Metal Complexes. *Inorganic Chemistry*, Vol.5, No.6, pp. 980–985.

Brooker, M. H. & Bates, J. B. (1971). Raman and Infrared Spectral Studies of Anhydrous Li_2CO_3 and Na_2CO_3. *The Journal of Chemical Physics*, Vol.54, No.11, pp. 4788–4796.

Buijs, K. & Schutte, C. J. H. (1961). The Infra-red Spectra and Structures of Li_2CO_3 and Anhydrous Na_2CO_3. *Spectrochimica Acta B*, Vol.17, No.9-10, pp. 927–932.

Burgio, N.; Iasonna, A; Magini, M.; Martelli, S. & Padella, F. (1991). Mechanical Alloying of the Fe-Zr System: Correlation between Input Energy and End Products. *Il Nuovo Cimento*, Vol.13D, No.4, pp. 459–476.

Busca, G. & Lorenzelli, V. (1982). Infrared Spectroscopic Identification of Species Arising from Reactive Adsorption of Carbon Oxides on Metal Oxide Surfaces. *Materials Chemistry*, Vol.7, No.1, pp. 89–126.

Cocco, G.; Delogu, F. & Schiffini, L. (2000). Toward a Quantitative Understanding of the Mechanical Alloying Process. *Journal of Materials Synthesis and Processing*, Vol.8, No.3-4, pp. 167–180.

Delogu, F. & Cocco, G. (2000). Relating Single-Impact Events to Macrokinetic Features in Mechanical Alloying Processes. *Journal of Materials Synthesis and Processing*, Vol.8, No.5-6, pp. 271–277.

Delogu, F.; Mulas, G.; Schiffini L. & Cocco, G. (2004). Mechanical Work and Conversion Degree in Mechanically Induced Processes. *Materials Science and Engineering A*, Vol.382, No.1-2, pp. 280–287.

El-Eskandarany, M. S.; Akoi, K.; Sumiyama, K. & Suzuki, K. (1997). Cyclic Crystalline-Amorphous Transformations of Mechanically Alloyed $Co_{75}Ti_{25}$. *Applied Physics Letters*, Vol.70, No.13, pp. 1679–1681.

Fujita, J.; Martell, A. E. & Nakamoto, K. (1962). Infrared Spectra of Metal Chelate Compounds. VIII. Infrared Spectra of Co(III) Carbonato Complexes. *The Journal of Chemical Physics*, Vol.36, No.2, pp. 339–345.

Gatehouse, B. M.; Livingstone, S. E. & Nyholm, R. S. (1958). The Infrared Spectra of Some Simple and Complex Carbonates. *Journal of the Chemical Society*, pp. 3137–3142.

Glinšek, S.; Malič, B.; Rojac, T.; Filipič, C.; Budič, B. & Kosec, M. (2011). $KTaO_3$ Ceramics Prepared by the Mechanochemically Activated Solid-State Synthesis. *Journal of the American Ceramic Society*, Vol.94, No.5, pp. 1368–1373.

Goldsmith, J. A. & Ross, S. D. (1967). Factors Affecting the Infra-Red Spectra of Planar Anions with D_{3h} Symmetry – IV. The Vibrational Spectra of Some Complex Carbonates in the Region 4000–400 cm^{-1}. *Spectrochimica Acta A*, Vol.24, No.8, pp. 993–998.

Haris, M. J. & Salje, E. K. H. (1992). The Incommensurate Phase of Sodium Carbonates: An Infrared Absorption Study. *Journal of Physics: Condensed Matter*, Vol.4, No.18, pp. 4399–4408.

Healy, P. C. & White, A. H. (1972). Crystal Structure and Physical Properties of Anhydrous Sodium Copper Carbonate. *Journal of the Chemical Society, Dalton Transactions*, pp. 1913–1917.

Hester, R. E. & Grossman, W. E. L. (1966). Vibrational Analysis of Bidentate Nitrate and Carbonate Complexes. *Inorganic Chemistry*, Vol.5, No.8, pp. 1308–1312.

Iasonna, A. & Magini, M. (1996). Power Measurements during Mechanical Milling: An Experimental Way to Investigate the Energy Transfer Phenomena. *Acta Materialia*, Vol.44, No.3, pp. 1109–1117.

Iguchi, Y. & Senna, M. (1985). Mechanochemical Polymorphic Transformation and Its Stationary State between Aragonite and Calcite. I. Effects of Preliminary Annealing. *Powder Technology*, Vol.43, No.2, pp. 155–162.

Jenko, D. (2006). *Synthesis of (K,Na)NbO_3 Ceramics*, PhD Thesis, University of Ljubljana, Ljubljana, Slovenia.

Jolivet, J. P.; Thomas, Y. & Taravel, B. (1980). Vibrational Study of Coordinated CO_3^{2-} Ions. *Journal of Molecular Structure*, Vol.60, pp. 93–98.

Jolivet, J. P.; Thomas, Y. & Taravel, B. (1982). Infrared Spectra of Cerium and Thorium Pentacarbonate Complexes. *Journal of Molecular Structure*, Vol.79, pp. 403–408.

Kong, L. B.; Zhang, T. S.; Ma, J. & Boey, F. (2008). Progress in Synthesis of Ferroelectric Ceramic Materials Via High-Energy Mechanochemical Technique. *Progress in Materials Science*, Vol.53, No.2, pp. 207–322.

Kuscer, D.; Holc, J. & Kosec, M. (2006). Mechano-Synthesis of Lead-Magnesium-Niobate Ceramics. *Journal of the American Ceramic Society*, Vol.89, No.10, pp. 3081–3088.

Le Brun, P.; Froyen, L. & Delaey, L. (1993). The Modeling of the Mechanical Alloying Process in a Planetary Ball Mill: Comparison between Theory and In-situ Observations. *Materials Science and Engineering A*, Vol. 161, No.1, pp. 75–82.

Liao, J. & Senna, M. (1992). Enhanced Dehydration and Amorphization of $Mg(OH)_2$ in the Presence of Ultrafine SiO_2 Under Mechanochemical Conditions. *Thermochimica Acta*, Vol.210, pp. 89–102.

Liao, J. & Senna, M. (1993). Mechanochemical Dehydration and Amorphization of Hydroxides of Ca, Mg and Al on Grinding With and Without SiO_2. *Solid State Ionics*, Vol.66, No.3-4, pp. 313–319.

Lin, I. J. & Nadiv, S. (1979). Review of the Phase Transformation and Synthesis of Inorganic Solids Obtained by Mechanical Treatment (Mechanochemical Reactions). *Materials Science and Engineering*, Vol.39, No.2, pp. 193–209.

Lu, L. & Lai, M. O. (1998). *Mechanical Alloying*, Kluwer Academic Publisher, Boston, USA.

Maurice, D. R. & Courtney, T. H. (1990). The Physics of Mechanical Alloying. *Metallurgical Transactions A*, Vol.21, No.1, pp. 289–303.

Nakamoto, K.; Fujita, J.; Tanaka, S. & Kobayashi, M. (1957). Infrared Spectra of Metallic Complexes. IV. Comparison of the Infrared Spectra of Unidentate and Bidentate Complexes. *Journal of the American Chemical Society*, Vol.79, No.18, pp. 4904–4908.

Nakamoto, K. (1997). *Infrared and Raman Spectra of Inorganic and Coordination Compounds. Part A: Theroy and Applications in Inorganic Chemistry*, Kluwer Academic Publisher, Boston, USA.

Rojac, T.; Kosec, M.; Šegedin, P.; Malič, B. & Holc, J. (2006). The Formation of a Carbonato Complex during the Mechanochemical Treatment of a Na_2CO_3–Nb_2O_5 Mixture. *Solid State Ionics*, Vol.177, No.33-34, pp. 2987–2995.

Rojac, T.; Benčan, A.; Uršič, H.; Malič, B. & Kosec, M. (2008a). Synthesis of a Li- and Ta-Modified (K,Na)NbO_3 Solid Solution by Mechanochemical Activation. *Journal of the American Ceramic Society*, Vol.91, No.11, pp. 3789–3791.

Rojac, T.; Kosec, M.; Malič, B. & Holc, J. (2008b). The Mechanochemical Synthesis of $NaNbO_3$ Using Different Ball-Impact Energies. *Journal of the American Ceramic Society*, Vol.91, No.5, pp. 1559–1565.

Rojac, T.; Kosec, M.; Polomska, M.; Hilczer, B.; Šegedin, P. & Benčan, A. (2009). Mechanochemical Reaction in the K_2CO_3–Nb_2O_5 System. *Journal of the European Ceramic Society*, Vol.29, No.14, pp. 2999–3006.

Rojac, T.; Benčan, A. & Kosec, M. (2010). Mechanism and Role of Mechanochemical Activation in the Synthesis of (K,Na,Li)(Nb,Ta)O_3 Ceramics. *Journal of the American Ceramic Society*, Vol.93, No.6, pp. 1619–1625.

Rojac, T.; Trtnik, Ž. & Kosec, M. (2011). Mechanochemical Reactions in Na_2CO_3–M_2O_5 (M = V, Nb, Ta) Powder Mixtures: Influence of Transition-Metal Oxide on Reaction Rate. *Solid State Ionics*, Vol.190, No.1, pp. 1–7.

Senna, M. & Isobe, T. (1997). NMR and EPR Studies on the Charge Transfer and Formation of Complexes through Incompletely Coordinated States. *Solid State Ionics*, Vol.101-103, No.1, pp. 387–392.

Sopicka-Lizer, M. (2010). *High-Energy Ball Milling: Mechanochemical Processing of Nanopowders,* Woodhead Publishing, Boston, USA.

Suryanarayana, C. (2001). Mechanical Alloying and Milling. *Progress in Materials Science*, Vol.46, No.3-4, pp. 1–184.

Tacaks, L. (2004). M. Carey Lea, The First Mechanochemist. *Journal of Materials Science*, Vol.39, No.16-17, pp. 4987–4993.

Tchernychova, E.; Glinšek, S.; Malič, B. & Kosec, M. (2011). Combined Analytical Transmission Electron Microscopy Approach to Reliable Composition Evaluation of $KTaO_3$. *Journal of the American Ceramic Society*, Vol.94, No.5, pp. 1611–1618.

Venyaminov, S. Y. & Pendergast, F. G. (1997). Water (H_2O and D_2O) Molar Absorptivity in the 1000–4000 cm^{-1} Range and Quantitative Infrared Spectroscopy of Aqueous Solutions. *Analytical Biochemistry*, Vol.248, No.2, pp. 234–245.

Wang, J.; Xue, J. M.; Wan, D. M. & Gan, B. K. (2000a). Mechanically Activating Nucleation and Growth of Complex Perovskites. *Journal of Solid State Chemistry*, Vol.154, No.2, pp. 321–328.

Wang, J.; Xue, J. M. & Wan, D. (2000b). How Different is Mechanical Activation from Thermal Activation? A Case Study with PZN and PZN-Based Relaxors. *Solid State Ionics*, Vol.127, No.1-2, pp. 169–175.

Watanabe, R.; Hashimoto, H. & Lee, G. G. (1995a). Computer Simulation of Milling Ball Motion in Mechanical Alloying (Overview). *Materials Transactions JIM*, Vol.36, No.2, pp. 102–109.

Watanabe, T.; Liao, J. & Senna, M. (1995b). Changes in the Basicity and Species on the Surface of Me$(OH)_2$–SiO_2 (Me=Ca, Mg, Sr) Mixtures Due to Mechanical Activation. *Journal of Solid State Chemistry*, Vol.115, No.2, pp. 390–394.

Watanabe, T.; Isobe, T. & Senna, M. (1996). Mechanisms of Incipient Chemical Reaction between $Ca(OH)_2$ and SiO_2 under Moderate Mechanical Stressing. I. A Solid State Acid-Base Reaction and Charge Transfer Due to Complex Formation. *Journal of Solid State Chemistry*, Vol.122, No.1, pp. 74–80.

Watanabe, T.; Isobe, T. & Senna, M. (1997). Mechanisms of Incipient Chemical Reaction between $Ca(OH)_2$ and SiO_2 under Moderate Mechanical Stressing. III. Changes in the Short-Range Ordering throughout the Mechanical and Thermal Processes. *Journal of Solid State Chemistry*, Vol.130, No.2, pp. 248–289.

Watters, R. L. (2005). NIST Standard Reference Database N°69, United States, June 2005 Release (robert.watters@nist.gov).

Zhang, Y. (1982). Electronegativities of Elements in Valence States and Their Applications. 1. Electronegativities of Elements in Valence States. *Inorganic Chemistry*, Vol.21, No.11, pp. 3886–3889.

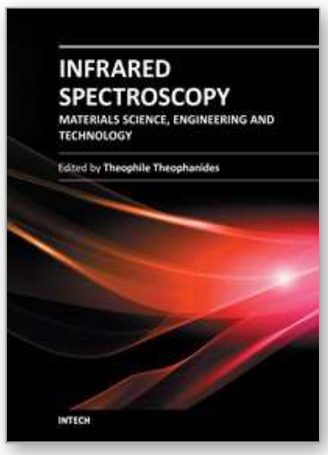

Infrared Spectroscopy - Materials Science, Engineering and Technology

Edited by Prof. Theophanides Theophile

ISBN 978-953-51-0537-4
Hard cover, 510 pages
Publisher InTech
Published online 25, April, 2012
Published in print edition April, 2012

The present book is a definitive review in the field of Infrared (IR) and Near Infrared (NIR) Spectroscopies, which are powerful, non invasive imaging techniques. This book brings together multidisciplinary chapters written by leading authorities in the area. The book provides a thorough overview of progress in the field of applications of IR and NIR spectroscopy in Materials Science, Engineering and Technology. Through a presentation of diverse applications, this book aims at bridging various disciplines and provides a platform for collaborations among scientists.

How to reference

In order to correctly reference this scholarly work, feel free to copy and paste the following:

Tadej Rojac, Primož Šegedin and Marija Kosec (2012). Using Infrared Spectroscopy to Identify New Amorphous Phases - A Case Study of Carbonato Complex Formed by Mechanochemical Processing, Infrared Spectroscopy - Materials Science, Engineering and Technology, Prof. Theophanides Theophile (Ed.), ISBN: 978-953-51-0537-4, InTech, Available from: http://www.intechopen.com/books/infrared-spectroscopy-materials-science-engineering-and-technology/using-infrared-spectroscopy-to-identify-new-amorphous-phases-a-case-study-of-carbonato-complexes-fo

INTECH
open science | open minds

InTech Europe
University Campus STeP Ri
Slavka Krautzeka 83/A
51000 Rijeka, Croatia
Phone: +385 (51) 770 447
Fax: +385 (51) 686 166
www.intechopen.com

InTech China
Unit 405, Office Block, Hotel Equatorial Shanghai
No.65, Yan An Road (West), Shanghai, 200040, China
中国上海市延安西路65号上海国际贵都大饭店办公楼405单元
Phone: +86-21-62489820
Fax: +86-21-62489821

IntechOpen